

The 2dF Galaxy Redshift Survey: the number and luminosity density of galaxies

Nicholas Cross,^{1*} Simon P. Driver,¹ Warrick Couch,² Carlton M. Baugh,³ Joss Bland-Hawthorn,⁴ Terry Bridges,⁴ Russell Cannon,⁴ Shaun Cole,³ Matthew Colless,⁵ Chris Collins,⁶ Gavin Dalton,⁷ Kathryn Deeley,² Roberto De Propriis,² George Efstathiou,⁸ Richard S. Ellis,⁹ Carlos S. Frenk,³ Karl Glazebrook,¹⁰ Carole Jackson,⁵ Ofer Lahav,⁸ Ian Lewis,⁴ Stuart Lumsden,¹¹ Steve Maddox,¹² Darren Madgwick,⁸ Stephen Moody,⁸ Peder Norberg,³ John A. Peacock,¹³ Bruce A. Peterson,⁵ Ian Price,⁵ Mark Seaborne,⁷ Will Sutherland,¹³ Helen Tadros⁷ and Keith Taylor⁴

¹*School of Physics and Astronomy, North Haugh, St Andrews, Fife KY16 9SS*

²*Department of Astrophysics, University of New South Wales, Sydney, NSW 2052, Australia*

³*Department of Physics, South Road, Durham DH1 3LE*

⁴*Anglo-Australian Observatory, PO Box 296, Epping, NSW 2121, Australia*

⁵*Research School of Astronomy and Astrophysics, The Australian National University, Weston Creek, ACT 2611, Australia*

⁶*Astrophysics Research Institute, Liverpool John Moores University, Twelve Quays House, Egerton Wharf, Birkenhead L14 1LD*

⁷*Department of Physics, Keble Road, Oxford OX1 3RH*

⁸*Institute of Astronomy, University of Cambridge, Madingley Road, Cambridge CB3 0HA*

⁹*Department of Astronomy, 105-24, California Institute of Technology, Pasadena, CA 91125, USA*

¹⁰*Department of Physics and Astronomy, John Hopkins University, Baltimore, MD 21218, USA*

¹¹*Department of Physics and Astronomy, E. C. Stoner Building, Leeds LS2 9JT*

¹²*School of Physics and Astronomy, University of Nottingham, University Park, Nottingham NG7 2RD*

¹³*Institute of Astronomy, University of Edinburgh, Royal Observatory, Edinburgh EH9 3HJ*

Accepted 2000 December 3. Received 2000 November 23; in original form 2000 May 18

ABSTRACT

We present the *bivariate brightness distribution* (BBD) for the 2dF Galaxy Redshift Survey (2dFGRS) based on a preliminary subsample of 45 000 galaxies. The BBD is an extension of the galaxy luminosity function, incorporating surface brightness information. It allows the measurement of the local luminosity density, j_B , and of the galaxy luminosity and surface brightness distributions, while accounting for surface brightness selection biases.

The recovered 2dFGRS BBD shows a strong luminosity–surface brightness relation [$M_B \propto (2.4 \pm_{0.5}^{1.5}) \mu_e$], providing a new constraint for galaxy formation models. In terms of the number density, we find that the peak of the galaxy population lies at $M_B \geq -16.0$ mag. Within the well-defined selection limits ($-24 < M_B < -16.0$ mag, $18.0 < \mu_e < 24.5$ mag arcsec⁻²) the contribution towards the luminosity density is dominated by conventional giant galaxies (i.e., 90 per cent of the luminosity density is contained within $-22.5 < M < -17.5$, $18.0 < \mu_e < 23.0$). The luminosity-density peak lies away from the selection boundaries, implying that the 2dFGRS is complete in terms of sampling the local luminosity density, and that luminous low surface brightness galaxies are rare. The final value we derive for the local luminosity density, inclusive of surface brightness corrections, is $j_B = 2.49 \pm 0.20 \times 10^8 h_{100} L_\odot \text{Mpc}^{-3}$. Representative Schechter function parameters are $M^* = -19.75 \pm 0.05$, $\phi^* = 2.02 \pm 0.02 \times 10^{-2}$ and $\alpha = -1.09 \pm 0.03$. Finally, we note that extending the conventional methodology to incorporate surface brightness selection effects has resulted in an increase in the luminosity density of ~ 37 per cent. Hence surface brightness selection effects would appear to explain much of the discrepancy between previous estimates of the local luminosity density.

* E-mail: njgc@st-andrews.ac.uk

Key words: surveys – galaxies: distances and redshifts – galaxies: general – galaxies: luminosity function, mass function.

1 INTRODUCTION

Of paramount importance in determining the mechanism(s) and epoch(s) of galaxy formation (as well as the local luminosity density) is the accurate and detailed quantification of the local galaxy population. It represents the benchmark against which both environmental and evolutionary effects can be measured. Traditionally this research area originated with the all-sky photographic surveys, coupled with a few handfuls of hard-earned redshifts. Over the past decade this has been augmented by both CCD-based imaging surveys and multislit/fibre-fed spectroscopic surveys. From these data, a number of perplexing problems have arisen, most notably the faint blue galaxy problem (Koo & Kron 1992; Ellis 1997), the local normalization problem (Maddox et al. 1990a; Shanks 1990; Driver, Windhorst & Griffiths 1995; Marzke et al. 1998), the cosmological significance of low surface brightness galaxies (LSBGs) (Disney 1976; McGaugh 1996; Sprayberry, Impey & Irvine 1996; Dalcanton et al. 1997; Impey & Bothun 1997) and dwarf galaxies (Babul & Rees 1992; Phillipps & Driver 1995; Babul & Ferguson 1996; Loveday 1997). These issues remain largely unresolved and arguably await an improved definition of the local galaxy population (Driver 1999).

Recent advancements in technology now allow for wide-field-of-view CCD imaging surveys¹ and bulk redshift surveys through purpose-built multifibre spectrographs such as the common-user two-degree field (2dF) facility at the Anglo-Australian Telescope (AAT) (Taylor, Cannon & Parker 1998). The Sloan Digital Sky Survey elegantly combines these two facets (Margon 1999).

The quantity and quality of data that are becoming available allow not only the revision of earlier results, but more fundamentally the opportunity to review and enhance the methodology with which the local galaxy population is represented. For instance, some criticism that might be levied at the current methodology – the representation of the space density of galaxies using the Schechter luminosity function (LF) (Schechter 1976; Felten 1985; Binggeli, Sandage & Tammann 1988) – is that, first, it assumes that galaxies are single-parameter systems defined by their apparent magnitude alone and, secondly, it describes the entire galaxy population by only three parameters: the characteristic luminosity L_* , the normalization of the characteristic luminosity ϕ_* , and the faint-end slope α . While it is desirable to represent the population with the minimum number of parameters, important information may lie in the nuances of detail.

In particular, two recent areas of research suggest a greater diversity in the galaxy population than is allowed by the Schechter function form. First, Marzke, Huchra & Geller (1994) and also Loveday (1997) report the indication of a change in the faint-end slope at faint absolute magnitudes – a possible giant–dwarf transition – and this is also seen in a number of Abell clusters where it is easier to probe into the dwarf regime (e.g. Driver et al. 1994; De Propris et al. 1995; Driver, Couch & Phillipps 1998; Trentham 1998). Secondly, a number of studies show that the three

¹ It is sobering to note that the largest published CCD-based imaging survey to date is 17.5 deg² to a central surface brightness of 25 V mag arcsec⁻² (Dalcanton et al. 1997) as compared to the all-sky coverage of photographic media.

Schechter parameters, and in particular the faint-end slope, have a strong dependence upon surface brightness limits (Sprayberry et al. 1996; Dalcanton 1998), colour (Lilly et al. 1996), spectral type (Folkes et al. 1999), optical morphology (Marzke et al. 1998), environment (Phillipps et al. 1998) and wavelength (Loveday 2000). It has been noted (Willmer 1997) that the choice of method for reconstructing the galaxy LF also contains some degree of bias.

More fundamentally, evidence that the current methodology might actually be flawed comes from comparing recent measurements of the galaxy LF as shown in Fig. 1. The discrepancy between these surveys is significantly adrift from the quoted formal errors, implying an unknown systematic error. The range of discrepancy can be quantified as a factor of 2 at the L_* ($M \sim -19.5$) point, rising to a factor of 10 at $0.01L_*$ ($M \sim -14.5$). The impact of this variation is a factor of 3–4, for instance, in assessing the contribution of galaxies to the local baryon budget (e.g. Persic & Salucci 1992; Bristow & Phillipps 1994; Fukugita, Hogan & Peebles 1998).

This uncertainty is in addition to that introduced from the unanswered question of the space density of LSBGs. The most recent attempt to quantify this is by O’Neil & Bothun (2000) – following on from McGaugh (1996), and in turn Disney (1976) – who conclude that the surface brightness function (SBF) of galaxies – the number density of galaxies in intervals of surface brightness – is of similar form to the LF. Thus both the LF and SBF are described by a flat distribution with a cut-off at bright absolute magnitudes or high surface brightnesses. Taking the O’Neil result at face value, this implies a further error in measures of the local luminosity density of 2–3 – i.e., the contribution to the luminosity (and hence baryon) density from galaxies is uncertain by a factor of ~ 10 . However, the significance of LSBGs depends upon their luminosity range, and similarly the

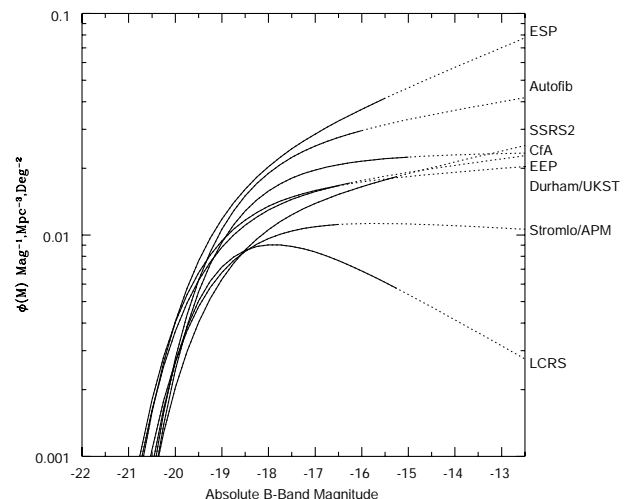


Figure 1. Schechter luminosity functions from recent magnitude-limited redshift surveys (see Table C1). The line becomes dotted outside the range of survey data. The range of values show the uncertainty in the LF, which in turn filters through to the local measure of the mean luminosity density.

completeness of the LF relies on the surface brightness intervals over which each luminosity bin is valid. Both representations are incomplete unless the information is combined. This leads us to the conclusion that both the total flux and the manner in which this flux is distributed must be dealt with simultaneously. Several papers have been published which deal with either surface brightness distributions or bivariate brightness distributions (BBDs) (Phillipps & Disney 1986; Sodre & Lahav 1993; Boyce & Phillipps 1995; Petrosian 1998; Minchin 1999). These are either theoretical, limited to cluster environments or have poor statistics due to the scarcity of good redshift data.

Recently, Driver (1999) determined the first measure of the BBD for field galaxies using Hubble Deep Field data (Williams et al. 1996) and capitalizing on photometric redshifts (Fernández-Soto, Lanzetta & Yahil 1999). The result, based on a volume-limited sample of 47 galaxies, implied that giant LSBGs were rare, but that there exists a strong luminosity–surface brightness relationship, similar to that seen in Virgo (Binggeli 1993). The sense of the relationship implied that LSBGs are preferentially of lower luminosity (i.e., dwarfs). If this is borne out, it strongly tempers the conclusions of O’Neil & Bothun (2000). While the number of LSBGs may be large, their luminosities are low, so their contribution to the local luminosity density is also low, <20 per cent (Driver 1999).

This paper attempts to bundle these complex issues on to a more intuitive platform by expanding the current representation of the local galaxy population to allow for surface brightness detection effects, star–galaxy separation issues, surface brightness photometric corrections, and clustering effects. This is achieved by expanding the monivariate LF into a bivariate brightness distribution (BBD), where the additional dimension is surface brightness. The 2dF Galaxy Redshift Survey (2dFGRS) allows us to do this for the first time by having a large enough data base to separate galaxies in both magnitude and surface brightness without having too many problems with small-number statistics.

In Section 2 we discuss the revised methodology for measuring the space density of the local galaxy population, the local luminosity density and the contribution towards the baryon density in detail. In Section 3 we present the current 2dFGRS data (containing ~45 000 galaxies, or one-fifth of the expected final tally). In Section 4 we correct for the light lost under the isophote, and define our surface brightness measure. In Section 5 we apply the methodology to construct the first statistically significant BBD for field galaxies. The results for the number density and luminosity density are detailed in Sections 6 and 7. In Section 8 we compare these results to other surveys. Finally, we present our conclusions in Section 9.

Throughout we adopt $H_0 = 100 \text{ km s}^{-1} \text{ Mpc}^{-1}$ and a standard flat cosmology with zero cosmological constant (i.e., $q_0 = 0.5$, $\Lambda = 0$). However, we note that the results presented here are only weakly dependent on the cosmology.

2 METHODOLOGY

The luminosity density, j , is the total amount of flux emitted by all galaxies per Mpc^3 . When measured in the UV band, it can be converted to a measure of the star formation rate (see, e.g., Lilly et al. 1996 and Madau, Della Valle & Panagia 1998). When measured at longer wavelengths, it can be combined with mass-to-light ratios to yield an *approximate* value for the contribution from galaxies towards the local matter density Ω_M – independent of H_0 , only weakly cosmology-dependent, and not reliant on any specific

theory of structure formation (see, e.g., Carlberg et al. 1996 and Fukugita et al. 1998). The two main caveats are, first, the accuracy of j_B (the luminosity density measured in the B -band) and, secondly, the assumption of a ubiquitous mass-to-light ratio.

2.1 Measuring j

The luminosity density, j , is found by integrating the product of the number density $\Phi(L/L_*)$ and the luminosity L with respect to luminosity:

$$j = \int_0^{\infty} L \Phi(L/L_*) d(L/L_*). \quad (1)$$

By convention, j is typically derived from a magnitude-limited redshift survey by determining the representative Schechter parameters for a survey (e.g. Efstathiou, Ellis & Peterson 1988) and then integrating the luminosity-weighted Schechter function, where $\Phi(L/L_*) d(L/L_*)$ is the Schechter function (Schechter 1976) given by

$$\Phi(L/L_*) d(L/L_*) = \phi_* (L/L_*)^\alpha \exp[-(L/L_*)] d(L/L_*), \quad (2)$$

where ϕ_* , L_* and α are the three parameters which define the survey (referred to as the normalization point, characteristic turn-over luminosity and faint-end slope parameter respectively). More simply, if a survey is defined by these three parameters, it follows that

$$j = \phi_* L_* \Gamma(\alpha + 2). \quad (3)$$

Table C1 shows values for the luminosity density derived from a number of recent magnitude-limited redshift surveys (as indicated). The variation between the measurements of j from these surveys is ~ 2 , and hence the uncertainty in the galaxy contribution to the mass budget is at best equally uncertain. This could be due to a number of factors, e.g., large-scale structure, selection biases, redshift errors, photometric errors or other incompleteness. In this paper we wish to explore the possibility of selection bias due to surface brightness considerations only. The principal motivation for this is that the LCRS (bottom line in Fig. 1), which recovers the lowest j value, adopted a bright isophotal detection limit of $\mu_r = 23 \text{ mag arcsec}^{-2}$, suggesting a dependence between the measured j and the surface brightness limit of the survey. Here we develop a method for calculating j which incorporates a number of corrections/considerations for surface brightness selection biases: in particular, a surface brightness-dependent Malmquist correction, a surface brightness redshift completeness correction, and an isophotal magnitude correction. We also correct for clustering. What is not included here, and will be pursued in a later paper, is the photometric accuracy, star–galaxy separation accuracy and a detection correction specifically for the 2dFGRS.

Implementing these corrections requires reformalizing the path to j . First, we replace the LF representation of the local galaxy population by a BBD. The BBD is the galaxy number density, Φ , as a function of absolute, total, B -band magnitude, M_B , and absolute, effective surface brightness, μ_e , i.e., $\Phi(M, \mu)$. To construct a BBD, we need to convert the observed distribution to a number density distribution, taking into account the Malmquist bias and the redshift incompleteness correction, i.e.,

$$\Phi(M, \mu) = \frac{O(M, \mu) + I(M, \mu)}{V(M, \mu)} W(M, \mu), \quad (4)$$

where:

(1) $O(M, \mu)$ is the matrix of absolute magnitude, M , and absolute effective surface brightness, μ , for galaxies with redshifts;

(2) $I(M, \mu)$ is the matrix of absolute magnitude, M , and absolute effective surface brightness, μ , for those galaxies for which redshifts were not obtained;

(3) $V(M, \mu)$ is the matrix which specifies the volume over which a galaxy with absolute magnitude, M , and absolute effective surface brightness, μ , can be seen (see also Phillipps, Davies & Disney 1990), and

(4) $W(M, \mu)$ is the matrix that weights each bin to compensate for clustering.

Deriving these matrices is discussed in detail later. j is then defined as

$$j = \sum^M \sum^\mu L(M)\Phi(M, \mu) \quad (5)$$

or, in practice,

$$j = \sum^M \sum^\mu 10^{-0.4(M-M_\odot)} \Phi(M, \mu) \quad (6)$$

in units of $L_\odot \text{Mpc}^{-3}$, where $M_{\odot B} = 5.48$.

Our formalism has two key advantages over the traditional luminosity function: First, it adds the additional dimensionality of surface brightness allowing for surface brightness specific corrections. Secondly, it represents the galaxy population by a distribution rather than a function, thus requiring no fitting procedures or assumption of any underlying parametric form.

3 THE DATA

The data set presented here is based upon a subsample of the Automated Plate Measuring-machine (APM) galaxy catalogue (Maddox et al. 1990a,b) for which spectra have been obtained using the 2dF facility at the AAT.

The original APM catalogue contains b_j magnitudes with random error $\Delta m = \pm 0.2$ mag (Folkes et al. 1999) and isophotal areas A_{ISO} . The isophotal area is defined as the number of pixels above a limiting isophote, μ_{lim} , set at the 2σ level above the sky background ($\mu_{\text{lim}} \approx 24.53 \text{ mag arcsec}^{-2}$ with a variation of $\pm 0.11 \text{ mag arcsec}^{-2}$; Pimblet et al. 2001). However, APM b_j magnitudes are found to vary from CCD b_j magnitudes by 0.14 ± 0.29 mag (Metcalf, Fong & Shanks 1995). Therefore the isophotal limit in APM b_j magnitudes is $\mu_{\text{lim}} = 24.67 \pm 0.30 \text{ mag arcsec}^{-2}$. One pixel equals 0.25 arcsec^2 . The minimum isophotal area found for galaxies in the APM catalogue is 35 arcsec^2 . Star–galaxy separation was implemented as described in Maddox et al. (1990b). The final APM sample contains 3×10^6 galaxies covering $15\,000 \text{ deg}^2$ (see Maddox et al. 1990a,b for further details).

The 2dFGRS input catalogue is a 2000 deg^2 subregion of the APM catalogue (covering two continuous regions in the northern and southern Galactic caps plus random fields) with an extinction-corrected magnitude limit of $m = 19.45$ (Colless 1999). The input catalogue contains 250 000 galaxies, for which 81 895 have been observed using 2dF (as of 1999 November). Each spectrum within the data base has been examined by eye to check if the redshift is reliable. Redshifts are determined via cross-correlation with specified templates (see Folkes et al. 1999 for details). A brief test of the reliability of the 2dFGRS was achieved via a comparison between 1404 galaxies in common with the Las

Campanas Redshift Survey (Lin et al. 1996), for which there were only eight mismatches, showing that 2dF redshifts are reliable. Of the 81 895 galaxies, 74 562 have a redshift, resulting in a redshift completeness of 91 per cent.

The survey comprises many overlapping two-degree fields, and many still have to be observed. Hence the absolute normalization is tied to the full input galaxy catalogue, which is known to contain 174.0 galaxies with $m \leq 19.45$ per square degree. Using a subsample of 44 796 galaxies, covering just the South Galactic Pole (SGP) region, this yields an *effective* coverage for this survey of 257 non-contiguous square degrees.

Finally, for the purposes of this paper, we adopt a lower redshift limit of $z = 0.015$ to minimize the influence of peculiar velocities in the determination of absolute parameters and an upper redshift limit of $z = 0.12$.

This upper limit of $z = 0.12$ was selected so as to maximize the sample size yet minimize the error introduced by the isophotal corrections. At $z = 0.12$ the uncertainty in the isophotal correction ($\pm_{0.16}^{0.07}$), due to type uncertainty (see Appendix A), remains smaller than the photometric error (± 0.2 mag). Note that the increase in the error in the isophotal correction is primarily because of the increase in the *intrinsic* isophotal limit due to a combination of surface brightness-dimming and the k -correction.

The final sample is therefore pseudo-*volume*-limited and contains 20 765 galaxies, with redshifts, selected from a parent sample of 45 000.

Note that all magnitude and surface brightnesses are in the APM b_j filter.

4 ISOPHOTAL CORRECTIONS

The APM magnitudes have already been corrected assuming a Gaussian profile (see Maddox et al. 1990b for full details). This was aimed primarily at recovering the light lost due to the seeing, and is crucial for compact objects. It is known to significantly underestimate the isophotal correction required for low surface brightness discs. Such systems typically exhibit exponential profiles with discs which can extend a substantial distance beyond the isophote, the most famous example being Malin 1 (Bothun et al. 1987). Once thought of as a Virgo dwarf, this system remains the most luminous field galaxy known.

To complement the Gaussian correction (required for compact objects but ineffectual for extended sources), we introduce an additional correction (ineffectual for compact sources but suitable for extended discs). This correction assumes all objects can be represented by a pure exponential surface brightness profile extending from the core outwards. In this case the surface brightness profile is simply

$$\Sigma(r) = \Sigma_o \exp(-r/\alpha), \quad (7)$$

or

$$\mu(r) = \mu_o + 1.086(r/\alpha), \quad (8)$$

where Σ_o is the central surface brightness in $\text{W m}^{-2} \text{arcsec}^{-2}$, α is the scalelength of the galaxy in arcsec, and r is the radius in arcsec. μ_o is the central surface brightness in mag arcsec^{-2} .

Under this assumption a galaxy's observed isophotal luminosity is the integrated radial profile out to r_{iso} :

$$l_{\text{iso}} = 2\pi \int_0^{r_{\text{iso}}} \Sigma_o \exp(-r/\alpha) r dr, \quad (9)$$

which can be expressed in magnitudes as

$$m_{\text{iso}} = \mu_o^{\text{app}} - 2.5 \log_{10} \{ 2\pi[\alpha^2 - \alpha(\alpha + r_{\text{iso}}) \exp(-r_{\text{iso}}/\alpha)] \} \quad (10)$$

(here μ_o^{app} denotes the apparent surface brightness uncorrected for redshift). μ_{lim} , the detection/photometry isophote, can be expressed as

$$\mu_{\text{lim}} = \mu_o^{\text{app}} + 1.086(r_{\text{iso}}/\alpha). \quad (11)$$

As m_{iso} , r_{iso} and μ_{lim} are directly measurable quantities, equations (10) and (11) can be solved numerically. The total magnitude is then given by

$$l_{\text{tot}} = 2\pi \int_0^{\infty} \Sigma_o \exp(-r/\alpha) r dr = 2\pi \Sigma_o \alpha^2, \quad (12)$$

or,

$$m^{\text{tot}} = \mu_o^{\text{app}} - 2.5 \log_{10}(2\pi\alpha^2) \quad (13)$$

From this description an extrapolated central surface brightness can be deduced numerically from the specified isophotal area and isophotal magnitude (after the seeing correction). Note that this prescription ignores the possible presence of a bulge, opacity, and inclination leading to an underestimate of the isophotal correction. This is unavoidable as the data quality is insufficient to establish bulge-to-disc ratios. To verify the impact of this, we explore the accuracy of the isophotal correction for a variety of galaxy types in Appendix A. The tests show that the isophotal correction is a significant improvement over the isophotal magnitudes for all types – apart from ellipticals where the introduced error is negligible compared to the photometric error – and a dramatic improvement for low surface brightness systems. The final magnitudes, after isophotal correction, now lie well within the quoted error of ± 0.2 mag for both high- and low-surface brightness galaxies.

4.1 The effective surface brightness

Most results cited in the literature use the central surface brightness or the effective surface brightness. The central surface brightness, as described above, is the extrapolated surface brightness at the core under the assumption of a perfect exponential disc. The effective surface brightness is the mean surface brightness within the half-light radius. The conversion between the measures is relatively straightforward and described as follows:

$$l_1 = \pi \Sigma_o \alpha^2 = 2\pi \Sigma_o \alpha^2 [1 - (1 + r_e/\alpha) \exp(-r_e/\alpha)], \quad (14)$$

which can be solved numerically to get

$$r_e = 1.678\alpha. \quad (15)$$

The effective surface brightness is now given by

$$\mu_e^{\text{app}} = \mu_o^{\text{app}} + 2.5 \log_{10}[(r_e/\alpha)^2] = \mu_o^{\text{app}} + 1.124. \quad (16)$$

Hence, from the isophotal magnitudes and areas we can derive the total magnitude and effective surface brightness (quantities which are now independent of the isophotal detection threshold). We chose to work with effective surface brightness as it can, at some later stage, be measured directly from higher quality CCD data. Note that these surface brightness measures are all *apparent* rather than *intrinsic*; however, this is not important as although surface brightness is distance-dependent, the isophotal correction is not

(this is because both μ_{lim} and μ_e vary with redshift in the same way).

Fig. 2 shows the final 2dFGRS sample (i.e., after isophotal correction) for those galaxies with (upper panel) and without (lower panel) redshifts. The galaxies are plotted according to their apparent total magnitude and apparent effective surface brightness. The curved boundary at the faint end of both plots is due to the isophotal corrections, which are strongly dependent on μ_e for a constant m . As $\mu_e - 1.124$ tends towards μ_{lim} , the isophotal limit, the correction tends towards infinity, making it impossible to see galaxies close to μ_{lim} . The average isophotal correction is 0.33 mag (for $\mu_{\text{lim}} = 24.67 \text{ mag arcsec}^{-2}$).

The observed mean magnitude and observed mean effective surface brightness for those galaxies with and without redshifts are

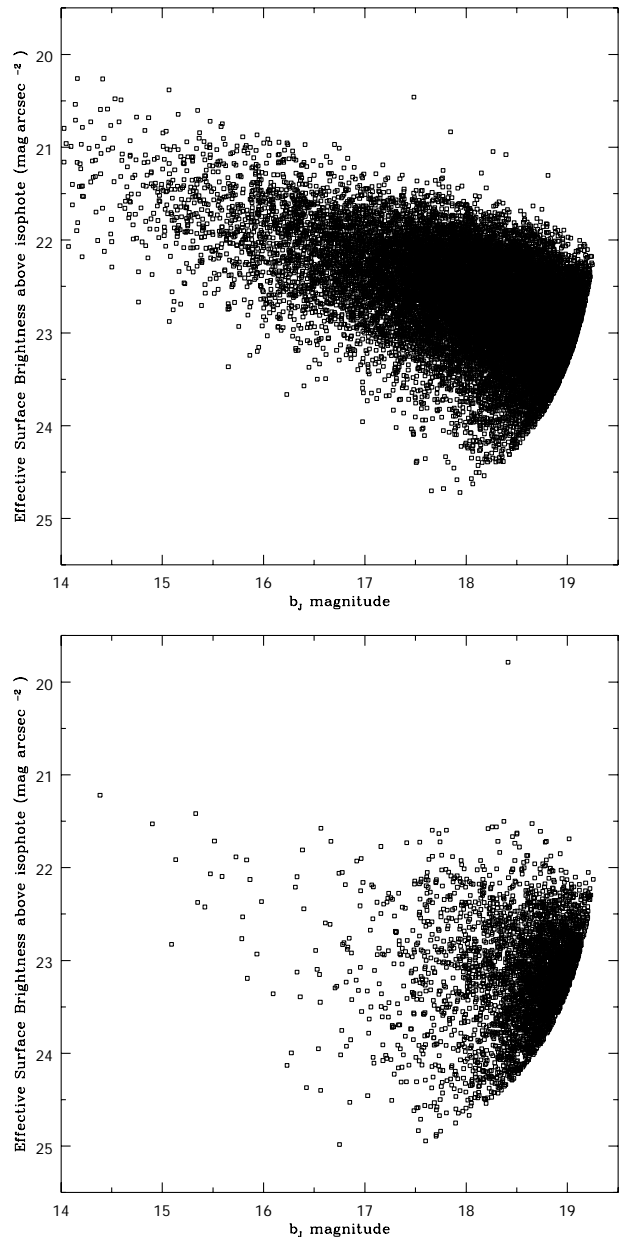


Figure 2. Galaxies with (upper) and without (lower) redshifts for the current 2dFGRS sample plotted according to their apparent extinction-corrected total magnitude and apparent effective surface brightness.

18.06 ± 0.01 mag and 22.66 ± 0.01 mag arcsec $^{-2}$, and 18.54 ± 0.01 mag and 23.17 ± 0.01 mag arcsec $^{-2}$, respectively. These figures imply that galaxies closer to the detection limits are preferentially undersampled.

5 CONSTRUCTING THE BBD

We now apply the methodology described in Section 2 to derive the BBD from our data set. This requires constructing the four matrices, $O(M, \mu)$, $I(M, \mu)$, $V(M, \mu)$ and $W(M, \mu)$.

5.1 Deriving $O(M, \mu)$

For those galaxies with redshifts, we can obtain their absolute magnitude and absolute effective surface brightness assuming a cosmological framework and a global k -correction,² $K(z) = 2.5z$ (Driver et al. 1994). The conversions from observed to absolute parameters are given by

$$M = m - 5 \log_{10} \left[\frac{2c}{H_0} (1+z)(1 - (1+z)^{-0.5}) \right] - 25 - K(z) \quad (17)$$

and

$$\mu_e = \mu_e^{\text{app}} - 10 \log_{10}(1+z) - K(z). \quad (18)$$

Here H_0 is the Hubble constant, c is the speed of light, μ_e^{app} is the apparent effective surface brightness, and μ_e is the absolute effective surface brightness. The M , derived by equation 17, is a total absolute magnitude, since the correction has been made for the light below the isophote.

Fig. 3 shows the upper panel of Fig. 2 with the axes converted to absolute parameter space using the conversions shown above. Naturally, galaxies in different regions are seen over differing volumes, because of Malmquist bias, hence it is not yet valid to compare the relative numbers. However, it is possible to define lines of constant volume, as shown in Fig. 3 (dotted lines). These lines are derived from visibility theory (Phillipps et al. 1990), and they delineate the region of the BBD plane where galaxies can be seen over various volumes. The shaded region shows the region where the volume is less than 10^4 Mpc^3 , and hence where we are insensitive to galaxy densities of $< 10^{-2} \text{ galaxies Mpc}^{-3} \text{ mag}^{-1} (\text{mag arcsec}^{-2})^{-1}$. The equations used to calculate the lines are laid out in Appendix B. We show a $V = 5 \times 10^5 \text{ Mpc}^3$ line rather than $V = 10^6 \text{ Mpc}^3$, because the $z = 0.12$ limit is at a volume less than $V = 10^6 \text{ Mpc}^3$. The parameters used in the visibility calculations are: $\mu_{\text{lim}} = 24.67 \text{ mag arcsec}^{-2}$; $\theta_{\text{min}} = 7.2 \text{ arcsec}$, $\theta_{\text{max}} = 200.0''$, $m_{\text{bright}} = 14.00 \text{ mag}$; $m_{\text{faint}} = 19.45 \text{ mag}$; $z_{\text{min}} = 0.015$, and $z_{\text{max}} = 0.12$. The clear space between the data and the selection boundary at bright absolute magnitudes implies that although the 2dFGRS data set samples a sufficiently representative volume ($V > 10000 \text{ Mpc}^3$), galaxies exist only over a restricted region of this observed BBD. Fainter than $M = -16.5 \text{ mag}$, the volume is insufficient to sample populations with a space density of $10^{-2} \text{ Mpc}^{-3} \text{ mag}^{-1} (\text{mag arcsec}^{-2})^{-1}$ or less.

Fig. 4 shows the data of Fig. 3 binned into μ_e and M intervals to produce the matrix $O(M, \mu)$ (see equation 4). The bins are $0.5 \text{ mag} \times 0.5 \text{ mag arcsec}^{-2}$ and start from -24.0 mag and a central surface brightness of $19.0 \text{ mag arcsec}^{-2}$, effective surface

² Individual k -corrections will be derived from the data; however, this has not yet been implemented.

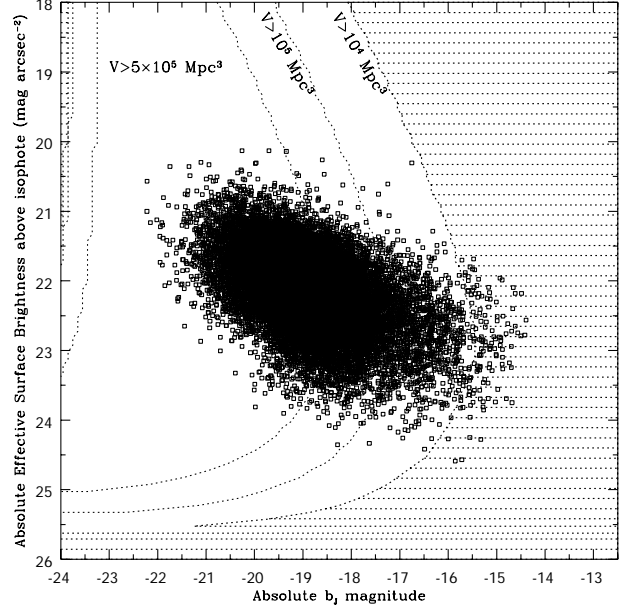


Figure 3. Galaxies from the 2dFGRS with redshifts, plotted in absolute magnitude and absolute effective surface brightness space. The shaded region denotes the regions where less than 10^4 Mpc^3 are surveyed, and is based on visibility theory as described in Phillipps, Davies & Disney (1990). The three curves represent the volumes of 10^4 , 10^5 and $5 \times 10^5 \text{ Mpc}^3$.

brightness of $20.12 \text{ mag arcsec}^{-2}$. The total number of bins is 200 in a uniform 20×10 array. Fig. 4 represents the *observed* distribution of galaxies, and shows a strong peak close to the typical M_* value seen in earlier surveys (see references listed in Table C1).

5.2 Deriving $I(M, \mu)$

Not all galaxies targeted by the 2dFGRS have a measured redshift. This may be due to lack of spectral features, selection biases or a misplaced/defunct fibre. One method to correct for these missing galaxies is to assume that they have the same observed BBD as those galaxies for which redshifts have been obtained. One can then simply scale up all bins by this known incompleteness.

However, from Fig. 2 and Sections 1 and 3 we noted that the incompleteness is a function of both the apparent magnitude and the apparent surface brightness. There is no reliable way of converting these values to absolute values without redshifts, and to obtain an incompleteness correction, $I(M, \mu)$, some assumption must be made. Here we assume that a galaxy of unknown redshift with apparent magnitude, m , and apparent effective surface brightness, μ_e , has a range of possible BBD bins that can be *statistically* represented by the BBD of galaxies with $m \pm \Delta m$ and $\mu_e \pm \Delta \mu_e$. The underlying assumption is that galaxies with and without redshifts with similar observed m and μ_e have similar redshift distributions, i.e., the detectability of a galaxy is primarily dependent on its apparent magnitude and apparent surface brightness. (While these factors are obviously crucial, one could also argue that additional factors, not incorporated here, such as the predominance of spectral features, are also important, so that the true probability distribution for the missing galaxies could be somewhat skewed from that derived in Fig. 5.)

Hence, for each galaxy without a redshift, we select those

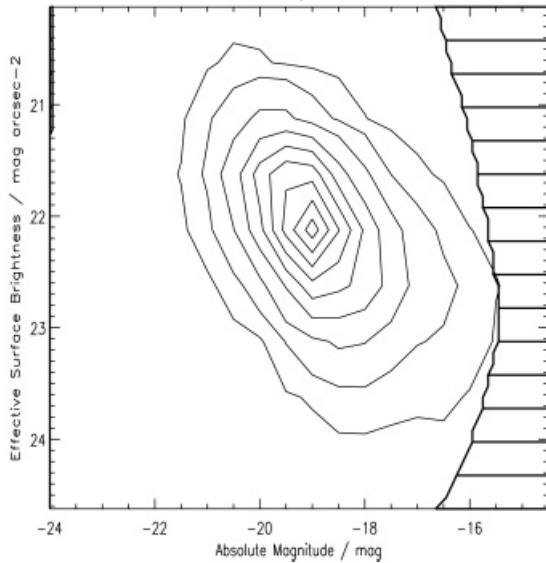
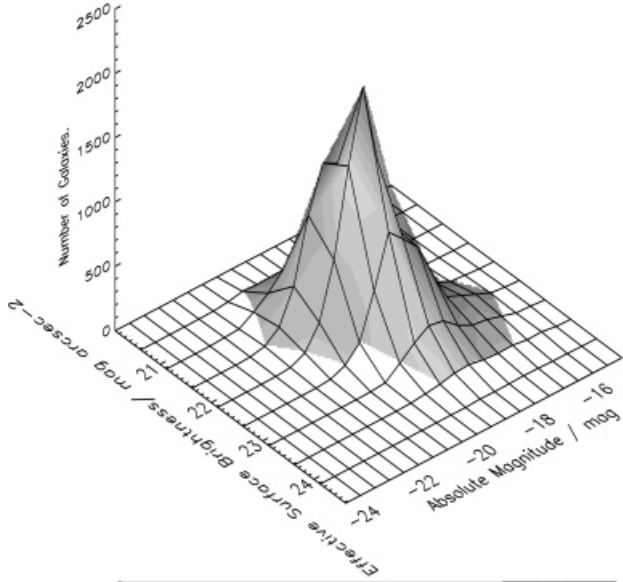


Figure 4. The observed distribution of the 2dFGRS data set mapped onto the BBD, prior to volume and incompleteness correction. The contour lines are set at 25, 100, 250, 500, 750, 1000, 1250, 1500 and 1750 galaxies per bin. The minimum number of galaxies in a bin is 25.

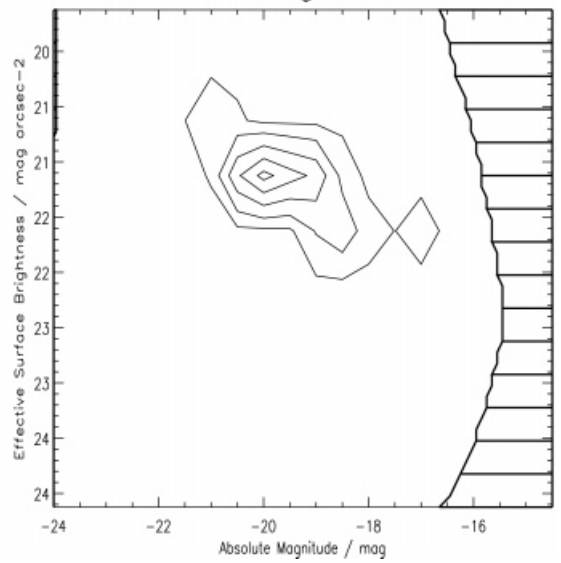
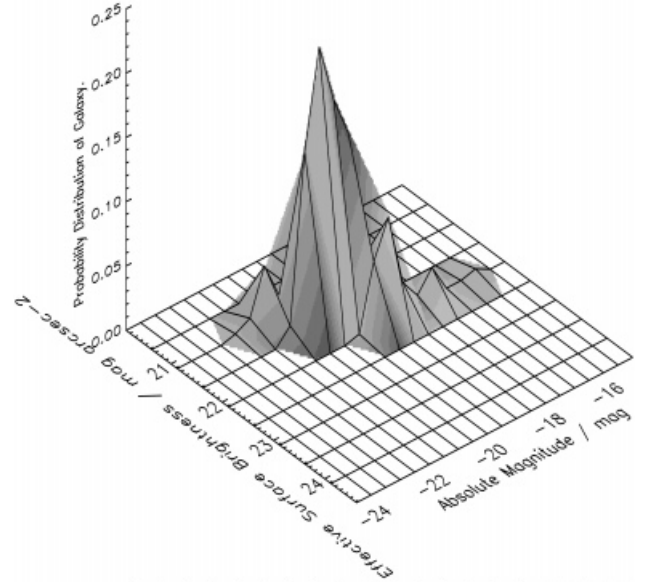


Figure 5. The BBD of galaxies with $m = 17.84 \pm 0.1$ and $\mu_e^{\text{app}} = 22.31 \pm 0.1$. The contour lines are set at 0.01, 0.05, 0.10, 0.15 and 0.20 chance of the galaxy being in that bin.

galaxies with redshifts within 0.1 mag and $0.1 \text{ mag arcsec}^{-2}$, and determine their collective observed BBD. This is achieved by using all 44 796 galaxies in the SGP sample, as galaxies without redshifts are not limited to $z < 0.12$. This distribution is then normalized to unity to generate a probability distribution for this galaxy. This is repeated for every galaxy without a redshift. Fig. 5 shows the probability distribution for a galaxy with $m = 17.839$ and $\mu_e = 22.314$. There are 317 galaxies with redshifts within 0.1 mag and $0.1 \text{ mag arcsec}^{-2}$, and combined they have a distribution ranging from $M = -15.44$ to $M = -21.76$ and $\mu_e = 22.26$ to $\mu_e = 21.06$.

To generate the matrix, $I(M, \mu)$, the probability distributions for each of the galaxies without redshifts (normalized to unity) are summed together to give the total distribution of those galaxies without redshifts. However, these galaxies could have the full range of redshifts that each galaxy can be detected over,

not a range limited to $z = 0.12$. Therefore the number distribution is weighted by the fraction of galaxies within each bin with $z < 0.12$.

Fig. 6 shows $I(M, \mu)$, which should be compared to Fig. 4 [$O(M, \mu)$]. The distribution of Fig. 6 appears broader, indicating that the missing galaxies are *not* random, but that they are predominantly low luminosity, low surface brightness systems. This is illustrated in Fig. 7, which shows the ratio of $I(M, \mu)$ to $O(M, \mu)$ for the bins containing more than 25 galaxies with redshifts. From Fig. 7 we see that the trend is for the ratio to increase towards the low surface brightness regime. There is no significant trend in absolute magnitude. Finally, we note that although the incompleteness correction does increase the population in some bins by as much as 50 per cent, we shall see in Sections 6 and 7 that the contribution from these additional systems towards the overall luminosity density is negligible.

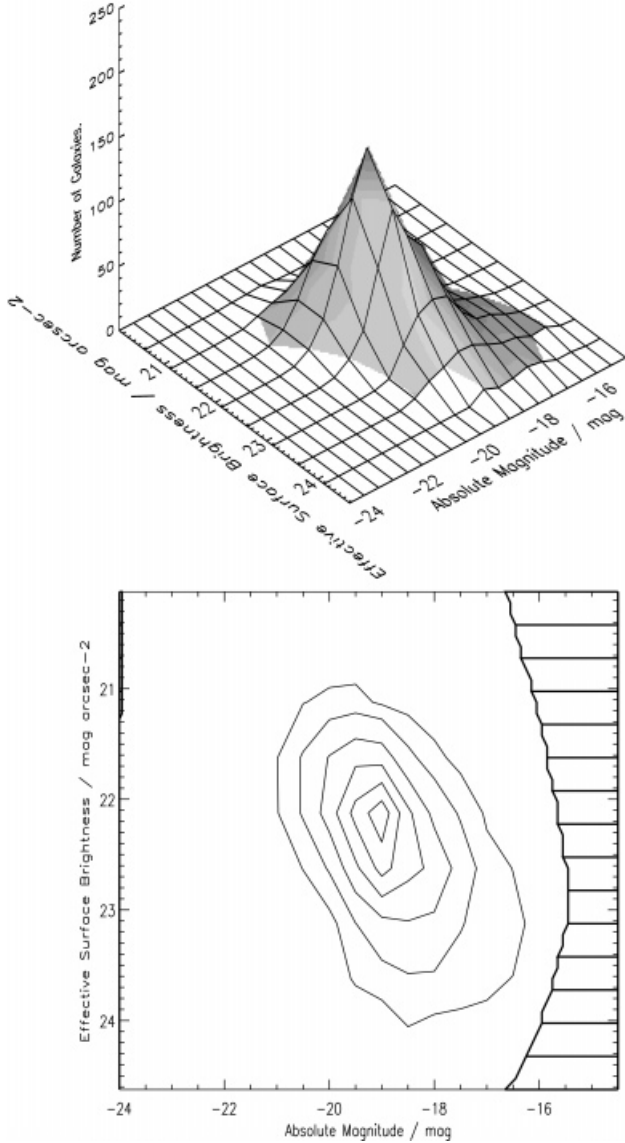


Figure 6. The bivariate number distribution of those galaxies without redshifts, i.e., $I(M, \mu)$. The contour lines are set at 10, 25, 50, 75, 100, 125 and 150 galaxies bin^{-1} .

5.3 Deriving $V(M, \mu)$

To convert the number of observed galaxies to number density per Mpc^3 , a Malmquist correction is required, i.e., $V(M, \mu)$. This matrix reflects the volumes over which each M, μ bin can be observed. One option is to use visibility theory as prescribed by Phillipps et al. (1990), and used to construct the constant volume line in Fig. 3. While visibility is clearly a step in the right direction, and preferable to applying a correction dependent on magnitude only, its limitation is that it assumes idealized galaxy profiles (i.e., it neglects the bulge component, seeing, star–galaxy separation and other complications). Ideally, one would like to extract the volume information from the data itself, and this is possible by using a $1/V_{\text{max}}$ type prescription, i.e., within each $O(M, \mu)$ bin, the maximum redshift at which a galaxy is seen is determined and the volume derived from this redshift. The advantages of using the data set rather than theory is that it naturally incorporates all redshift-dependent selection biases.

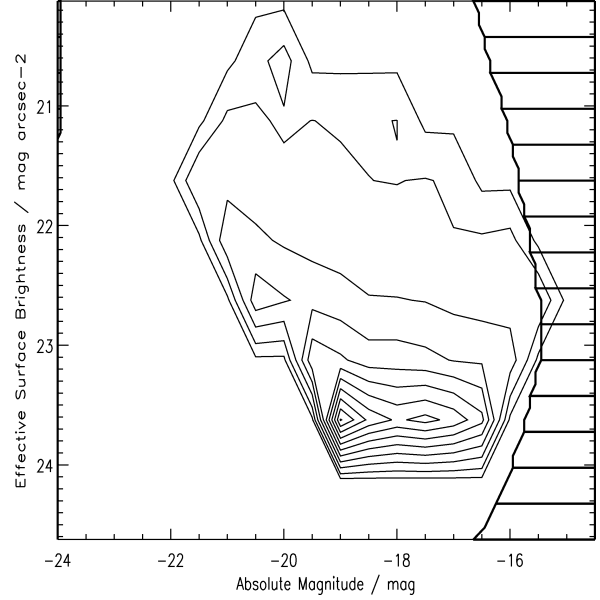


Figure 7. The ratio of galaxies without redshifts to galaxies with redshifts. The contour lines are set at 0.01, 0.05, 0.10, 0.15, 0.20, 0.25, 0.30, 0.35, 0.40, 0.45 and 0.50.

However, the maximum redshift is susceptible to scattering from higher visibility bins. An improved version is therefore to use the 90th percentile redshift, and to adjust $O(M, \mu)$ and $I(M, \mu)$ accordingly.

Although this requires rejecting 10 per cent of the data, it has two distinct advantages. First, it ensures that the redshift distribution in each bin has a sharp cut-off (as opposed to a distribution which tapers out). Secondly, it uses the entire data set as opposed to the maximum redshift only. In the case where the 90th percentile is not exact, we take the galaxy nearest. Using these redshifts, the volume can be calculated independently for each bin, assuming an Einstein–de Sitter cosmology as follows:

$$V(M, \mu) = V_{z_{\min}(M, \mu)}^{z_{90}(M, \mu)}, \quad (19)$$

where

$$V_{z_{\min}(M, \mu)}^{z_{90}(M, \mu)} = \int_{z_{\min}(M, \mu)}^{z_{90}(M, \mu)} \frac{\sigma d_l^2}{H_0(1+z)^{3.5}} dz, \quad (20)$$

and σ is the solid angle in steradians on the sky. d_l is the luminosity distance to the galaxy, and z_{\min} is the minimum distance over which a galaxy can be detected. z_{\min} is calculated from visibility theory (Phillipps et al. 1990; see also Appendix B), adopting values for the maximum magnitude and maximum size of $m_B = 14.00$ mag and $\theta = 200$ arcsec respectively.

Fig. 8 shows the matrix $\frac{1}{V(M, \mu)}$. Note that squares containing fewer than 25 galaxies are not shaded. This matrix is flat-bottomed due to the cut-off at $z = 0.12$. Fig. 8 shows a strong dependency upon magnitude (i.e., classical Malmquist bias as expected) and also upon surface brightness. This surface brightness dependency is particularly strong near the 10^4Mpc^3 volume limit, as the data become sparse. Inside this volume limit the contour lines generally mimic the curve of the visibility-derived volume boundary. This suggests that visibility theory provides a good description of the combined volume dependency. The sharp cut-off along the high surface brightness edge may be real, but it could also be a manifestation of the complex star–galaxy

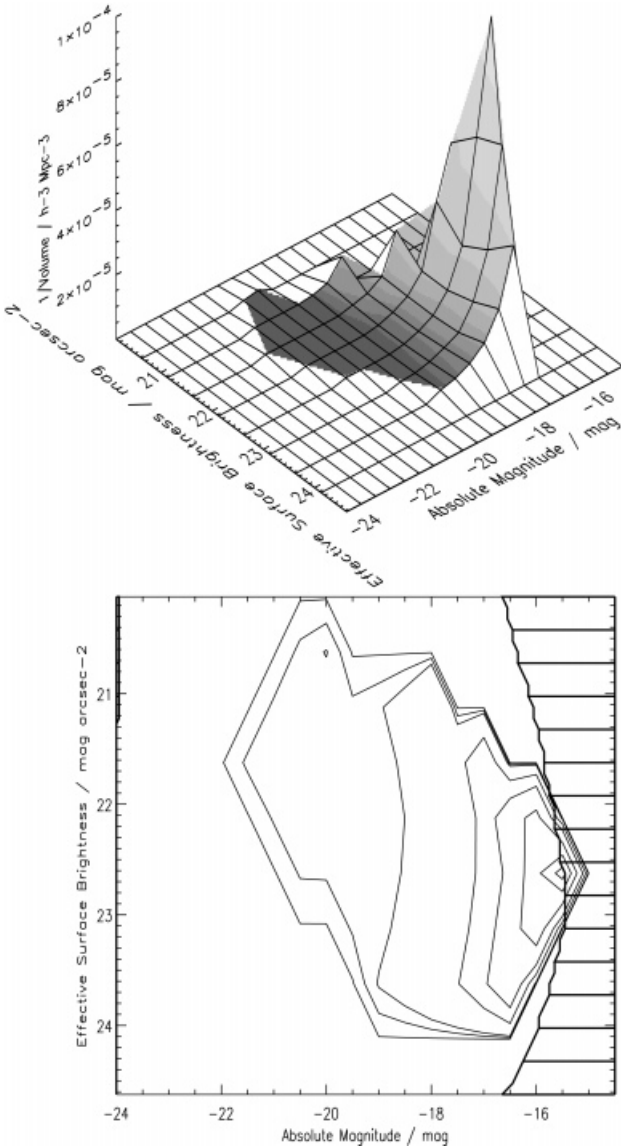


Figure 8. Plot of $1/\text{volume}$ in each bin. The contour lines are set at 1.0×10^{-7} , 1.0×10^{-6} , 2.0×10^{-6} , 1.0×10^{-5} , 2.0×10^{-5} , 4.0×10^{-5} , 6.0×10^{-5} , 8.0×10^{-5} and $1.0 \times 10^{-4} h^{-3} \text{Mpc}^{-3}$.

separation algorithm (see Maddox et al. 1990a). Given that a galaxy seen over a larger distance appears more compact, and that local dwarfs have smaller scalelengths than giants (cf. Mateo 1998), this seems reasonable. We will investigate this further through high-resolution imaging.

The main point to take away from Fig. 8 is that the visibility surface of the 2dFGRS input catalogue is complex and dependent on both M and μ_e (though predominantly M). Any methodology which ignores surface brightness information and implements a volume-bias correction in luminosity only is implicitly assuming uniform visibility in surface brightness. The 2dFGRS data clearly show that this is not the case.

5.4 Clustering

Structure is seen on the largest measurable scales (e.g. de Lapparent, Geller & Huchra 1986). To determine whether the effects of clustering are significant, we constructed a radial

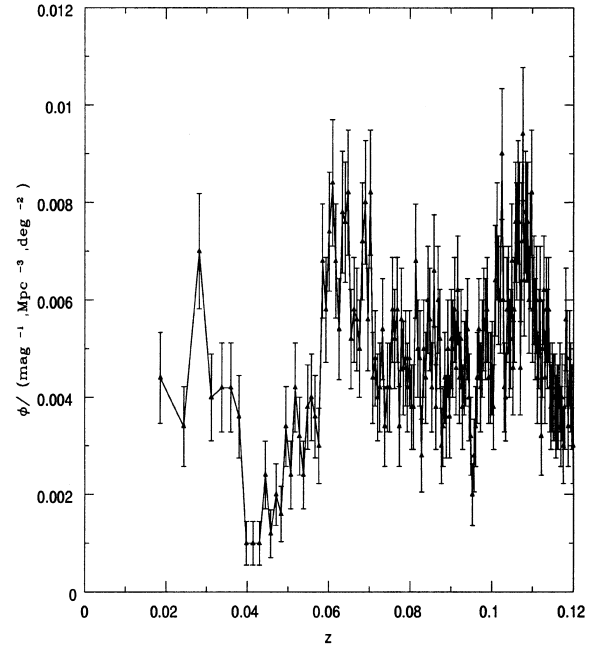


Figure 9. The clustering map. This shows the number density of giant galaxies ($-19.75 < M < -18.75$ and $21.1 < \mu_e < 22.6$) as a function of redshift. The points are spaced equally in volume at intervals of $5000 h^3 \text{Mpc}^3$, starting at $10000 h^3 \text{Mpc}^3$.

density profile, as shown in Fig. 9. This was derived from those bins for which more than 100 galaxies are seen over the whole range from $0.015 < z < 0.12$ (i.e., $-19.75 < M < -18.75$ and $21.1 < \mu_e < 22.6$). Those galaxies which are brighter cannot be seen at $z < 0.015$ due to the bright-magnitude cut-off at $m = 14.00$, and would therefore bias the number density towards the bright end. For these high-visibility galaxies we calculated their number density (ϕ) in equal volume intervals of $5.0 \times 10^3 \text{Mpc}^3$, from $z = 0.0185$ to 0.12 . Fig. 9 shows that clustering is severe, with what appears to be a large local void around $z = 0.04$ and walls at $z = 0.06$ and 0.11 . The ESO Slice Project (ESP) survey (Zucca et al. 1997), whose line of sight (RA $\sim 00\text{h}$, Dec. ~ -40) is just outside the 2dF SGP region, measures an underdensity at $\leq 140 h^{-1} \text{Mpc}$ ($z \approx 0.045$) and an overdensity at $z \approx 0.1$. The structure that they see closely resembles the structure that we see. A reliable measure of the BBD needs to correct for this clustering bias. Here we adopt a strategy which implicitly assumes, first, that clustering is independent of either M or μ , and, secondly, that evolutionary processes to $z = 0.12$ are negligible.

On the basis of these caveats, we constructed a weighting matrix, $W(M, \mu)$. This was determined from the high-visibility galaxies by taking the ratio of the number density of high-visibility galaxies over the full redshift range divided by the number density of high-visibility galaxies over the redshift range of each bin, i.e.,

$$W(M, \mu) = \frac{\bar{\phi}(\text{High} - \text{vis})_{z=0.015}^{z=0.12}}{\phi(\text{High} - \text{vis})_{z_{\min}(M, \mu)}^{z_{\max}(M, \mu)}}. \quad (21)$$

This weighting matrix is shown in Fig. 10. The implication is that the number density of low-luminosity systems will be amplified by almost a factor of 1.5, to correct for the apparent presence of a large local void along the SGP region – indicated by the vertical ridge at $M = -17$ in Fig. 10. Once again, this

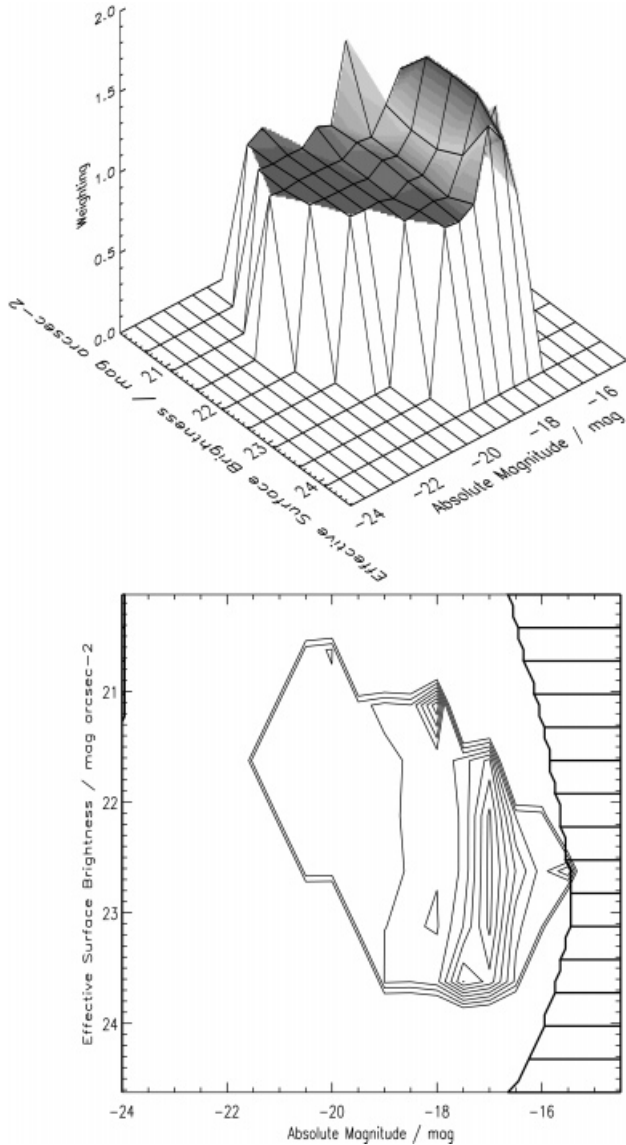


Figure 10. The weighting map. The contours are at 0.8, 0.9, 1.0, 1.1, 1.2, 1.3, 1.4 and 1.5.

implicitly assumes that the clustering of dwarf and giant systems is correlated.

6 THE 2DFGRS BBD

Finally, we can combine the four matrices, $O(M, \mu)$, $I(M, \mu)$, $V(M, \mu)$ and $W(M, \mu)$ (see equation 4), to generate the 2dFGRS bivariate brightness distribution, as shown in Fig. 11. This depicts the underlying local galaxy number density distribution, inclusive of surface brightness selection effects. Only those bins which are based upon 25 or more galaxies are shown. Note that by summing the BBD along the surface brightness axis, one recovers the luminosity distribution of galaxies. By summing along the magnitude axis, one obtains the surface brightness distribution of galaxies (see Section 8).

Fig. 12 shows the errors in the BBD. These were initially determined via Monte Carlo simulations, assuming a Gaussian error distribution of ± 0.2 mag in the APM magnitudes. This showed that the errors were proportional to $\sqrt{(1/N)}$ and, since

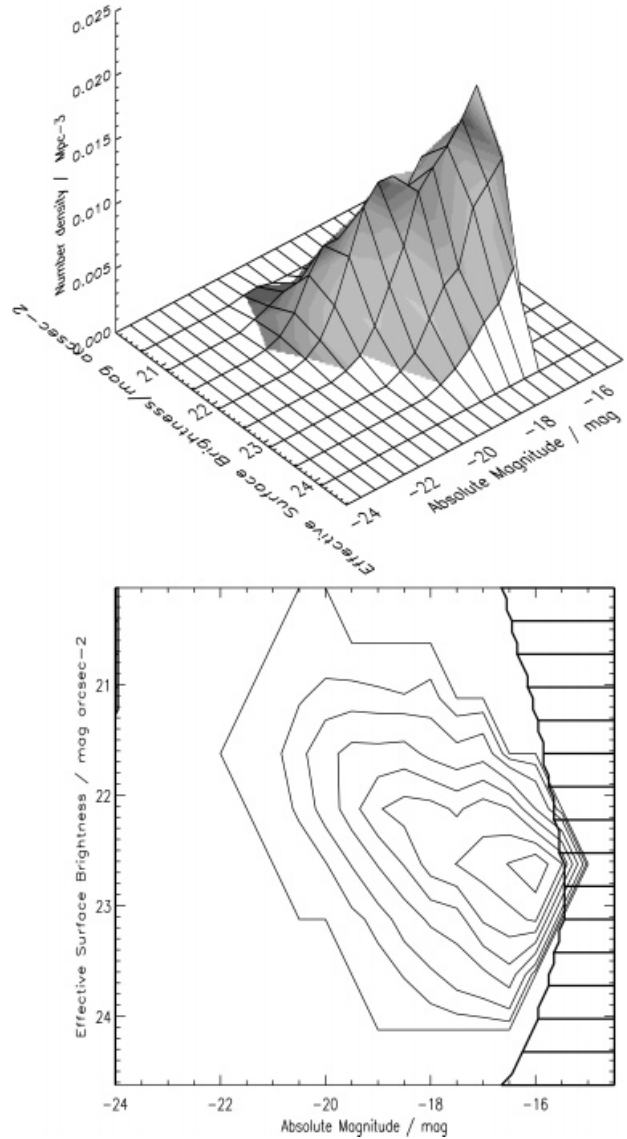


Figure 11. The 2dFGRS bivariate brightness distribution. The contour lines are set at 1.0×10^{-7} , 1.0×10^{-3} , 2.5×10^{-3} , 5.0×10^{-3} , 7.5×10^{-3} , 1.0×10^{-2} , 1.25×10^{-2} , 1.5×10^{-2} , 1.75×10^{-2} , 2.0×10^{-2} , and 2.25×10^{-2} galaxies $\text{Mpc}^{-3} \text{bin}^{-1}$. The thick lines represent the selection boundaries calculated from visibility theory.

$\sqrt{(1/N)}$ is much faster to calculate, this is the result that is used throughout the calculations. These errors were then combined in quadrature with the additional error in the volume estimate, assuming Poisson statistics. The total error is given by

$$\sigma_{\phi} = \sqrt{\left[\frac{1}{N_{\text{tot}}(M, \mu)} \right]^2 + \left[\frac{1}{N_z(M, \mu)} \right]^2}. \quad (22)$$

The errors become significant (> 20 per cent) when $M > -16$ and around the boundaries of the BBD shown in Fig. 11. The data and associated errors are tabulated in Table C2. From Figs 11 and 12 we note the following.

6.1 A luminosity–surface brightness relation

The BBD shows evidence of a luminosity–surface brightness

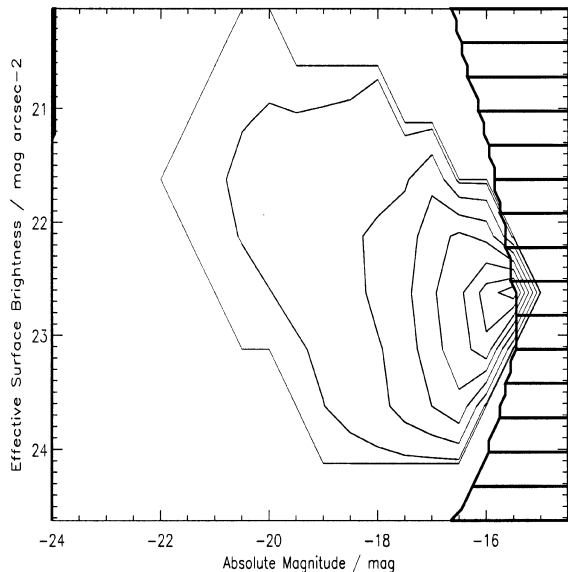


Figure 12. The errors in the BBD. The contour lines are set at 1.0×10^{-7} , 1.0×10^{-4} , 5.0×10^{-4} , 1.0×10^{-3} , 1.5×10^{-3} , 2.0×10^{-3} , 2.5×10^{-3} , 3.0×10^{-3} , 3.5×10^{-3} and 4.0×10^{-3} galaxies $\text{Mpc}^{-3} \text{bin}^{-1}$.

relation similar to that seen in Virgo ($M_B \propto 1.6\mu_o$; Binggeli 1993) in the Hubble Deep Field ($M_{F450W} \propto 1.5\mu_e$; Driver 1999) and in Sdm galaxies ($M_B \propto 2.02 \pm 0.16\mu_e$; de Jong & Lacey 2000). A formal fit to the 2dFGRS data yields $M_B \propto (2.4 \pm_{0.5}^{1.5})\mu_e$. While confirming the general trend, this result appears significantly steeper than the Virgo and HDF results. Both the Virgo and HDF results are based on lower luminosity systems, and so this might be indicative of a second-order dependency of the relation upon luminosity. Alternatively, it may reflect slight differences in the data/analysis, as neither the Virgo nor HDF data include isophotal corrections, whereas the 2dFGRS data are more susceptible to atmospheric seeing. The gradient is slightly steeper than the de Jong & Lacey result, but is well within the errors.

The presence of a luminosity–surface brightness relation highlights concerns over the completeness of galaxy surveys, as surveys with bright isophotal limits will preferentially exclude dwarf systems, leading to an underestimate of their space densities and variations such as those seen in Fig. 1.

The confirmation of this luminosity–surface brightness relation within such an extensive data set is an important step forward, and any credible model of galaxy formation must now be required to reproduce this relation.

6.2 A dearth of luminous, low surface brightness galaxies

Within each magnitude interval there appears to be a preferred range in surface brightness over which galaxies may exist. While the high surface brightness limit *may* be due, in part or whole, to star–galaxy separation and/or fibre-positioning accuracy, the low surface brightness limit appears to be real. It cannot be a selection limit, as one requires a mechanism which hides luminous LSBGs yet allows dwarf galaxies of similar surface brightness to be detected within the same volume. The implications are that these galaxy types (luminous LSBGs) are rare, with densities less than 10^{-4} galaxies Mpc^{-3} . This result is important, as it directly addresses the issues raised in the introduction, and implies that existing surveys have *not* missed large populations of luminous

LSBGs. Perhaps more importantly, it confirms that the 2dFGRS is complete for giant galaxies, and that the postulate that the Universe might be dominated by luminous LSBGs (Disney 1976) is ruled out.

One caveat, however, is that luminous LSBGs could be masquerading as dwarfs. For example, consider the case of Malin 1 (Bothun et al. 1987), which has a huge extended disc (55 kpc scalelength) of very low surface brightness ($\mu_o = 26.5$). This system is actually readily detectable because of its high surface brightness active core; however, within the 2dFGRS limits it would have been misclassified as a dwarf system with $M = -17.9$, $\mu_e = 21.8$. Hence Figs 11 and 12 rule out luminous disc systems only. To determine whether objects such as Malin 1 are hidden amongst the dwarf population will require either ultra-deep CCD imaging or cross-correlation with H I-surveys which would exhibit very high H I mass-to-light ratios for such systems.

6.3 The rising dwarf population

The galaxy population shows a steady increase in number density with decreasing luminosity. This continues to the survey limits at $M = -16$, whereupon the volume limit and surface brightness selection effects impinge upon our sample. The expectation is that the distribution continues to rise, and hence the location of the peak in the number density distribution remains unknown. However, we do note that the increase seen within our selection limits is insufficient for the dwarf population to dominate the luminosity density, as shown in the next section.

Perhaps more surprising is the lack of substructure, indicating either a continuity between the giant and dwarf populations or that any substructure is erased by the random errors. The former case is strongly indicative of a hierarchical merger scenario for galaxy formation which one expects to lead towards a smooth number density distribution between the dwarf and giant systems (White & Rees 1978). This is contrary to the change in the luminosity distribution of galaxies seen in cluster environments (e.g. Smith, Driver & Phillipps 1997). In a later paper we intend to explore the dependency of the BBD upon environment.

7 THE VALUE OF j_B AND Ω_M

The luminosity density matrix $j(M, \mu)$ is constructed from $L\Phi(M, \mu)$ in units of $L_\odot \text{Mpc}^{-3}$, and is shown as Fig. 13. The distribution is strongly peaked close to the conventional M_* parameter derived in previous surveys (see Table C1). The peak lies at $M = -19.5$ mag and $\mu_e = 22.12$ mag arcsec $^{-2}$. The final value obtained is $j_B = (2.49 \pm 0.20) \times 10^8 h_{100} L_\odot \text{Mpc}^{-3}$. The sharp peak sits firmly in the centre of our observable region of the 2dFGRS BBD, and drops rapidly off on all sides towards the 2dFGRS BBD boundaries. This implies that while the 2dFGRS does not survey the entire parameter space of the known BBD, it does effectively contain the full galaxy contribution to the local luminosity density. Redoing the calculations using galaxies with redshifts also results in $j_B = (2.49 \pm 0.20) \times 10^8 h_{100} L_\odot \text{Mpc}^{-3}$. This demonstrates that there is no dependency of the results upon the assumption made for the distribution of galaxies without redshifts.

We note that j derived via a direct $1/V_{\text{max}}$ estimate, without any surface brightness or clustering corrections, (equation 1) gives a value of $j = 1.82 \pm 0.07 \times 10^8 h_{100} L_\odot \text{Mpc}^{-3}$. Including the isophotal magnitude correction only leads to a value of

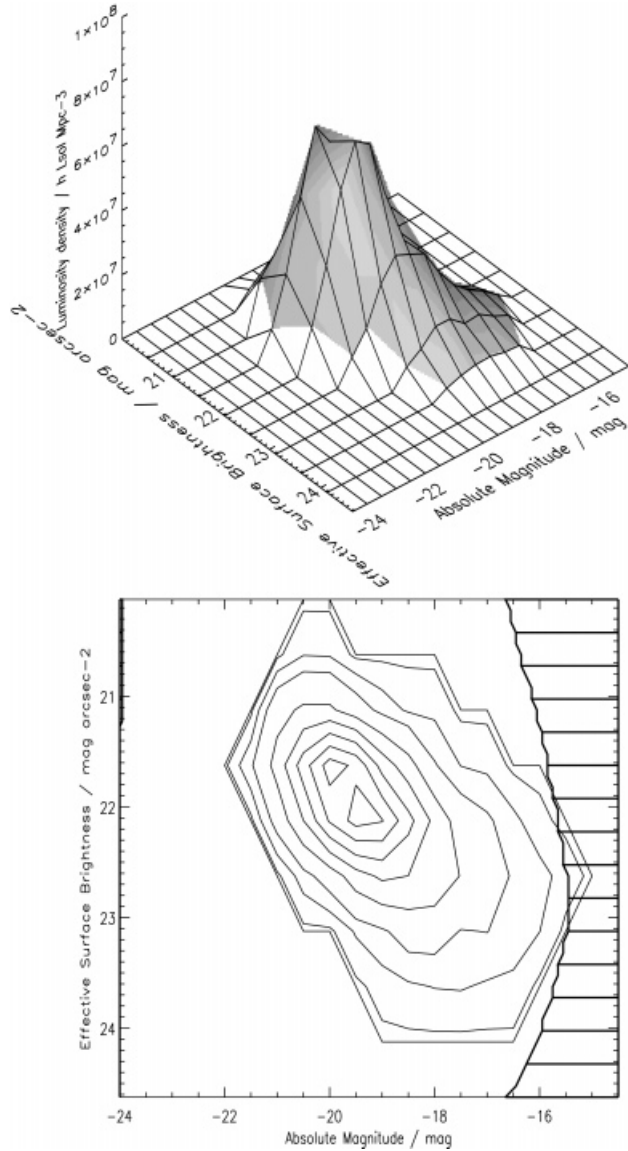


Figure 13. Plot of the luminosity density distribution. The contour lines are set at 100, 1.0×10^6 , 5.0×10^6 , 1.0×10^7 , 2.0×10^7 , 3.0×10^7 , 4.0×10^7 , 5.0×10^7 and $6.0 \times 10^7 L_{\odot} \text{Mpc}^{-3} \text{bin}^{-1}$.

$j = 2.28 \pm 0.09 \times 10^8 h_{100} L_{\odot} \text{Mpc}^{-3}$. Hence a more detailed analysis leads to a 36.8 per cent increase in j , of which 25.3 per cent is due to the isophotal correction, 10.4 per cent is due to the Malmquist bias correction, and 1.1 per cent is due to the clustering correction.

The final value agrees well with that obtained from the recent ESO Slice Project (Zucca et al. 1997). The method that they used corrects for clustering, but not surface brightness – although their photometry is based on aperture rather than isophotal magnitudes. However, it is worth pointing out that j is sensitive to the exact value of μ_{lim} . The quoted error in μ_{lim} is ± 0.3 (for plate-to-plate variations, see Metcalfe et al. 1995 and Pimblett et al. 2000). Table C3 shows a summary of results when repeating the entire analysis using the upper and lower error limits. It therefore seems likely that a combination of surface brightness biases and large-scale structure can indeed lead to the type of variations seen in Table C1.

Finally, following the method of Carlberg, Yee & Ellingson

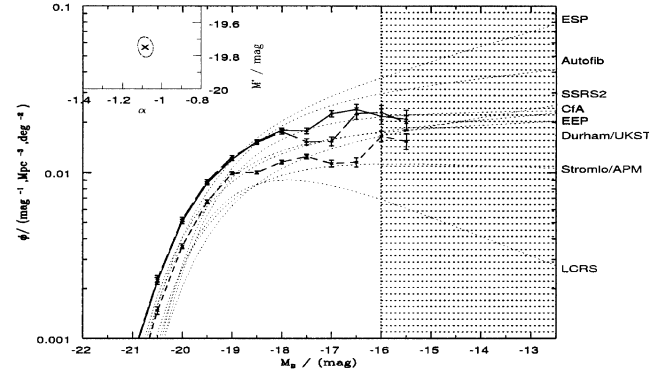


Figure 14. The solid line shows the final luminosity function, with all corrections taken into account. The long-dashed line shows the LF with surface brightness corrections only, and the short-dashed line shows the LF ignoring surface brightness and clustering corrections. Also shown, as dotted lines, are the LFs from Fig. 1. The shaded region denotes the limit of reliability based on visibility theory.

(1997), we can obtain a crude ball-park figure for the total local mass density by adopting a universal mass-to-light ratio based on that observed in clusters. While this method neglects biasing (White, Tully & Davis 1988), it does provide a useful crude upper limit to the mass density. From Carlberg et al. (1997) we find: $\mathcal{M}_{\text{Dyn}}/L_R = 289 \pm 50 h_{100} M_{\odot}/L_{\odot}$. Assuming a mean colour of $(B - R) = 1.1$ and a solar colour index of 1.17, this converts to: $\mathcal{M}_{\text{Dyn}}/L_B = 271 \pm 47 h_{100} M_{\odot}/L_{\odot}$. Multiplying the luminosity density by the mass-to-light ratio yields a value for the local mass density of $\Omega_M \approx 0.24$. We note that this is consistent with the current constraints from the combination of SN Ia results with the recent Boomerang and Maxima-1 results (Balbi et al. 2000; de Bernardis et al. 2000).

8 COMPARISONS WITH OTHER SURVEYS

As this work represents the first detailed measure of the field BBD, there is no previous work with which to compare. However, as mentioned earlier, it is trivial to convert the BBD into either a luminosity distribution and/or a surface brightness distribution, both of which have been determined by numerous groups. This is achieved by summing across either luminosity or surface brightness intervals. For those bins containing fewer than 25 galaxies for which a volume- and clustering-bias correction were not obtained we use the volume-bias correction from the nearest bin with 25 or more galaxies. This will lead to a slight underestimate in the number-densities; however, as the number density peak is well defined, this effect is negligible.

8.1 The luminosity distribution

Fig. 14 shows a compendium of luminosity function measures (see Table C1 and Fig. 1). Superimposed on the previous Schechter function fits (dotted lines) are the results from the 2dFGRS. Three results are shown, the luminosity distribution neglecting surface brightness and clustering (short-dashed line), the luminosity distribution inclusive of surface brightness corrections (long-dashed line), and finally the luminosity distribution inclusive of surface brightness and clustering corrections (solid line). The inset shows the $2\sigma\chi^2$ error ellipse for the last case, yielding Schechter function parameters of $M_{*} = -19.75 \pm 0.05$, $\alpha = -1.09 \pm 0.03$

and $\phi_* = 0.0202 \pm 0.0002$, in close agreement with the ESO Slice Project (ESP) (see Table C1).

Comparing the 2dFGRS result with other surveys suggests that the main effects of the surface brightness correction are to shift M_* brightwards by the mean isophotal correction of 0.33 mag and to increase the number density by a factor of 1.2. The clustering correction has little effect at bright magnitudes, almost by definition, but significantly amplifies the dwarf population. This is a direct consequence of an apparent local void at $z = 0.04$ along the full range of the 2dF SGP region.

We note that the combination of these two corrections closely mimics the discrepancies between various Schechter function fits. For example, the shallower SSRS2, APM and Durham/UKST surveys are biased at all magnitudes by the apparent local void, while the deeper ESP and Autofib surveys (which employ clustering independent methods) probe beyond the void. Similarly, because of the luminosity–surface brightness relation, those surveys which probe to lower surface brightnesses will yield higher dwarf-to-giant ratios.

The shaded region shows the point at which our data start to become highly uncertain because of the small volume surveyed ($V < 10\,000 \text{ Mpc}^3$). As this is the first statistically significant investigation into the bivariate brightness distribution, we can conclude that as yet no survey contains any direct census of the space density of $M_B > -16.0 \text{ mag}$ galaxies.

8.2 The surface brightness distribution

There have been a few surface brightness functions (SBFs) published over the years. The first was the Freeman (1970) result, which showed a Gaussian distribution with $\bar{\mu} = 21.65$ and $\sigma_\mu = 0.3$. Since then, however, many galaxies have been found at greater than 10σ from the mean. The probability of a galaxy occurring at 10σ or greater is $\approx 1 \times 10^{-20}$. The total number of galaxies in the Universe is in the range of 10^{11} – 10^{12} , so the Freeman SBF must be underestimating the LSBGs. The distribution seen by Freeman is almost certainly due to the relatively bright isophotal detection threshold that the observations were taken at, around 22 – $23 \text{ mag arcsec}^{-2}$. A more recent measure of the SBF comes from O’Neil & Bothun (2000), who also show a

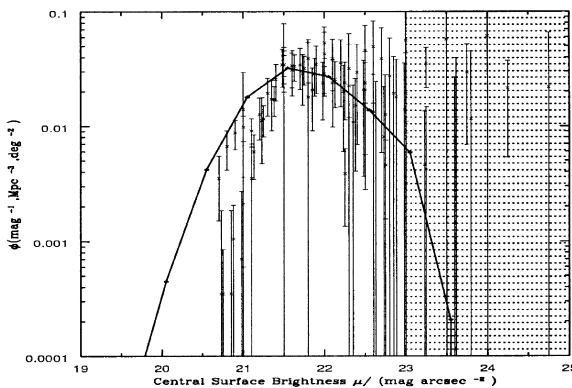


Figure 15. The solid line shows the final surface brightness function, with all the surface brightness and clustering corrections. The points are offset towards the low surface brightness direction by 0.55 mag to crudely correct for the bulge. Also shown are the O’Neil & Bothun (2000) data, as crosses with error bars. The shaded region is where the visibility line shown in the previous diagrams starts to cross the data, and so the data are no longer completely reliable.

compendium of results from other groups. The O’Neil & Bothun data, in contrast to the Freeman result, show a flat distribution over the range $22 < \mu_o < 25$, albeit with substantial scatter. Fig. 15 reproduces fig. 1. of O’Neil & Bothun, but now includes the final 2dFGRS results. In order to compare our results directly with the O’Neil & Bothun data, we assumed a mean bulge-to-total ratio of 0.4 (see Kent 1985), resulting in a uniform offset of $0.55 \text{ mag arcsec}^{-2}$.

The 2dFGRS data are substantially broader than the Freeman distribution, and appear to agree well with the compendium of data summarized in O’Neil & Bothun (2000). From visibility theory (see Fig. 3) our data are complete (i.e., the volume observed is greater than 10^4 Mpc^3 and therefore statistically representative) in central surface brightness from $18.0 < \mu_o < 23$ for $M < -16$. Assuming that the luminosity–surface brightness relation continues as reported in Driver (1999) and Driver & Cross (2000), the expectation is that the surface brightness distribution will steepen as galaxies with lower luminosities are included.

9 CONCLUSIONS

We have introduced the bivariate brightness distribution (BBD) as a means by which the effect of surface brightness selection biases in large galaxy catalogues can be investigated. By correcting for the light below the isophote and including a surface brightness-dependent Malmquist correction, we find that the measurement of the luminosity density is increased by ~ 37 per cent over the traditional $1/V_{\text{max}}$ method of evaluation. The majority (25 per cent) of this increase comes from the isophotal correction, with 10 per cent due to incorporating a surface brightness-dependent Malmquist correction, and 1 per cent due to the clustering correction.

We have shown that our isophotal correction is suitable for all galaxy types, and that isophotal magnitudes without correction severely underestimate the magnitudes for specific galaxy types. We also note that the redshift incompleteness suggests that predominantly low surface brightness galaxies are being missed; however, we also show that these systems are predominantly low-luminosity and hence contribute little to the overall luminosity density. This is in part due to the high completeness of the 2dFGRS (~ 91 per cent).

We rule out the possibility of the 2dFGRS missing a significant population of luminous giant galaxies down to $\mu_e = 24.5 \text{ mag arcsec}^{-2}$ (or $\mu_o = 23.5 \text{ mag arcsec}^{-2}$), and note that the contribution at surface brightness limits below $\mu_e = 23 \text{ mag arcsec}^{-2}$ is small and declining. Dwarf galaxies greatly outnumber the giants, and the peak in the number density occurs at the low-luminosity selection boundary. The implication is that the most numerous galaxy type lies at $M > -16.0 \text{ mag}$. The galaxy population as a whole follows a luminosity–surface brightness relation [$M \propto (2.4 \pm_{0.5}^{1.5}) \mu_e$] similar (but slightly steeper) to that seen in Virgo, in the Hubble Deep Field and in SdM galaxies. This relation provides an additional constraint which galaxy formation models must satisfy.

We conclude that our measure of the galaxy contribution to the luminosity density is robust and dominated by conventional giant galaxies, with only a small (< 10 per cent) contribution from dwarf ($M > -17.5 \text{ mag}$) and/or low surface brightness giants ($\mu_e > 23 \text{ mag arcsec}^{-2}$) within the selection boundaries ($-24 < M_B < -15.5 \text{ mag}$, $18.0 < \mu_e < 24.5 \text{ mag arcsec}^{-2}$). However, we cannot rule out the possibility of a contribution from an

independent population outside of our optical selection boundaries.

Our measurement of the luminosity density is $j = 2.49 \pm 0.20 \times 10^8 h_{100} L_{\odot} \text{Mpc}^{-3}$, and using a typical cluster mass-to-light ratio leads to an estimate of the matter density of order $\Omega_M \sim 0.24$, in agreement with more robust measures.

Finally, we note that the bivariate brightness distribution offers a means of studying the galaxy population and luminosity density as a function of environment and epoch fully inclusive of surface brightness selection biases. Future extensions to this work will include the measurement of BBDs and ‘population peaks’ for individual spectral/morphological types, and as a function of redshift and environment. This step forward has become possible only because of the recent availability of large redshift survey data bases such as that provided by the 2dFGRS.

ACKNOWLEDGMENTS

The data shown here were obtained via the two-degree field facility on the 3.9-m Anglo-Australian Observatory. We thank all those involved in the smooth running and continued success of the 2dF and the AAO.

REFERENCES

- Babul A., Ferguson H. C., 1996, *ApJ*, 458, 100
 Babul A., Rees M., 1992, *MNRAS*, 255, 346
 Balbi A. et al., 2000, *ApJ*, 545, L1
 Beijersbergen M., de Blok W. J. G., van der Hulst J. M., 1999, *A&A*, 351, 903
 Binggeli B., 1993, in Meylan G., Prugniel P., eds, *ESO/OHP Workshop on Dwarf Galaxies*. ESO, Garching, p. 13
 Binggeli B., Sandage A., Tammann G. A., 1988, *ARA&A*, 26, 509
 Bothun G. D., Impey C. D., Malin D. F., Mould J. R., 1987, *AJ*, 94, 23
 Boyce P. J., Phillipps S., 1995, *A&A*, 296, 26
 Bristow P. D., Phillipps S., 1994, *MNRAS*, 267, 13
 Carlberg R. G., Yee H. K. C., Ellingson E., Abraham R., Gravel P., Morris S., Pritchet C. J., 1996, *ApJ*, 462, 32
 Carlberg R. G., Yee H. K. C., Ellingson E., 1997, *ApJ*, 478, 462
 Colless M., 1999, *Phil. Trans. R. Soc.*, 357, 105
 Dalcanton J. J., 1998, *ApJ*, 495, 251
 Dalcanton J. J., Spergel D. N., Gunn J. E., Schmidt M., Schneider D. P., 1997, *AJ*, 114, 635
 de Bernardis P. et al., 2000, *Nat*, 404, 955
 de Propriis R., Pritchet C. J., Harris W. E., McClure R. D., 1995, *ApJ*, 450, 534
 de Jong R., Lacey C., 2000, *ApJ*, 545, 781
 de Lapparent V., Geller M. J., Huchra J. P., 1986, *ApJ*, 304, 585
 de Vaucouleurs G., 1948, *Ann. Astrophys.*, 11, 247
 Disney M., 1976, *Nat*, 263, 573
 Disney M., Phillipps S., 1983, *MNRAS*, 205, 1253
 Driver S. P., 1999, *ApJ*, 526, L69
 Driver S. P., Cross N. J. G., 2000, in Kraan-Korteweg R., Henning P., Andernach H., eds, *ASP Conf. Ser. Vol. 218, Mapping the Hidden Universe*. Kluwer, Dordrecht, p. 309
 Driver S. P., Phillipps S., Davies J. I., Morgan I., Disney M. J., 1994, *MNRAS*, 266, 155
 Driver S. P., Windhorst R. A., Griffiths R. E., 1995, *ApJ*, 453, 48
 Driver S. P., Couch W. J., Phillipps S., 1998, *MNRAS*, 301, 369
 Efstathiou G., Ellis R., Peterson B., 1988, *MNRAS*, 232, 431
 Ellis R. S., 1997, *ARA&A*, 35, 389
 Ellis R. S., Colless M., Broadhurst T., Heyl J., Glazebrook K., 1996, *MNRAS*, 280, 235
 Felten J. E., 1985, *Comments Astrophys.*, 11, 53
 Ferguson H. C., Binggeli B., 1994, *A&AR*, 6, 67
 Fernández-Soto A., Lanzetta K., Yahil A., 1999, *ApJ*, 513, 34
 Folkes S. et al., 1999, *MNRAS*, 308, 459
 Freeman K., 1970, *ApJ*, 160, 811
 Fukugita M., Hogan C. J., Peebles P. J. E., 1998, *ApJ*, 503, 518
 Gaztanaga E., Dalton G. B., 2000, *MNRAS*, 312, 417
 Impey C., Bothun G., 1997, *ARA&A*, 35, 267
 Kent S. M., 1985, *ApJS*, 59, 115
 Koo D. C., Kron R. G., 1992, *ARA&A*, 30, 613
 Lilly S. J., Le Fèvre O., Hammer F., Crampton D., 1996, *ApJ*, 460, 1
 Lin H., Kirshner R., Shectman S., Landy S., Oemler A., Tucker D., Schechter P., 1996, *ApJ*, 464, 60
 Loveday J., 1997, *ApJ*, 489, 29
 Loveday J., 2000, *MNRAS*, 312, 557
 Loveday J., Peterson B. A., Efstathiou G., Maddox S. J., 1992, *ApJ*, 390, 338
 Madau P., Della Valle M., Panagia N., 1998, *ApJ*, 498, 106
 Maddox S. J., Sutherland W. J., Efstathiou G., Loveday J., 1990a, *MNRAS*, 243, 692
 Maddox S. J., Efstathiou G., Sutherland W. J., 1990b, *MNRAS*, 246, 433
 Margon B., 1999, *Phil. Trans. R. Soc.*, 357, 105
 Marzke R., Huchra J., Geller M., 1994, *ApJ*, 428, 43
 Marzke R., Da Costa N., Pelligrini P., Willmer C., Geller M., 1998, *ApJ*, 503, 617
 Mateo M. L., 1998, *ARA&A*, 36, 435
 McGaugh S. S., 1996, *MNRAS*, 280, 337
 Metcalfe N., Fong R., Shanks T., 1995, *MNRAS*, 274, 769
 Minchin R. F., 1999, *Publ. Astron. Soc. Aust.*, 16, 12
 O’Neil K., Bothun G. D., 2000, *ApJ*, 529, 811
 Persic M., Salucci P., 1992, *MNRAS*, 258, 14p
 Petrosian V., 1998, *ApJ*, 507, 1
 Phillipps S., Disney M., 1986, *MNRAS*, 221, 1039
 Phillipps S., Driver S. P., 1995, *MNRAS*, 274, 832
 Phillipps S., Davies J., Disney M., 1990, *MNRAS*, 242, 235
 Phillipps S., Driver S. P., Couch W. J., Smith R. M., 1998, *ApJ*, 498, L119
 Pimblet K. A., Smail I., Edge A. C., Couch W. J., O’Hely E., Zabludoff A. I., 2001, *MNRAS*, submitted
 Ratcliffe A., Shanks T., Parker Q., Fong R., 1998, *MNRAS*, 293, 197
 Schechter P., 1976, *ApJ*, 203, 297
 Shanks T., 1990, in Bowyer S. C., Leinert C., eds, *Proc. IAU Symp. 139, Extragalactic Background Radiation*. Kluwer, Dordrecht, p. 269
 Smith R. M., Driver S. P., Phillipps S., 1997, *MNRAS*, 287, 415
 Smoker J. V., Axon D. J., Davies R. D., 1999, *A&A*, 341, 725
 Sodre L., Jr, Lahav O., 1993, *MNRAS*, 260, 285
 Sprayberry D., Impey C., Irwin M., 1996, *ApJ*, 463, 535
 Taylor K., Cannon R. D., Parker Q., 1998, in McLean B. J., Golembek D. A., Haynes J. J. E., Payne H. E., eds, *Proc. IAU Symp. 179, New Horizons from Multi Wavelength Sky Surveys*. Kluwer, Dordrecht, p. 135
 Trentham N., 1998, *MNRAS*, 294, 193
 van den Bergh S., 1998, *Galaxy Morphology and Classification*. Cambridge Univ. Press, Cambridge
 Williams R. E. et al., 1996, *AJ*, 112, 1335
 Willmer C. N. A., 1997, *AJ*, 114, 898
 White S. D. M., Rees M. J., 1978, *MNRAS*, 183, 341
 White S. D. M., Tully B., Davis M., 1988, *ApJ*, 333, L45
 Zucca E. et al., 1997, *A&A*, 326, 477

APPENDIX A: TESTING THE ISOPHOTAL CORRECTIONS

It is possible to model several different types of galaxy, and to compare the isophotal magnitude and the total magnitude as calculated in Section 4 with the ‘true’ magnitude. The models are simple, assuming a face on circular galaxy, and composed of a bulge with a de Vaucouleurs $r^{\frac{1}{4}}$ law (de Vaucouleurs 1948) and a

disc with an exponential profile (see equation 8):

$$\mu_{\text{bulge}} = \mu_e + 1.40 + 8.325[(r/r_e)^{1/4} - 1], \quad (\text{A1})$$

where r_e is the half-light radius of the bulge, and μ_e is the effective surface brightness of the bulge. Here we define μ_e as the mean surface brightness within r_e .³ However, it is more useful to define galaxies in terms of their luminosities and bulge-to-disc ratios than their effective radii or disc scalelengths.

The magnitude of a galaxy and the bulge-to-disc ratio can be found in terms of the above parameters by

$$M = -2.5 \log_{10}(10^{-0.4B} + 10^{-0.4D})$$

$$B/T = \frac{B}{B+D} = \frac{1}{1 + 1/\left(\frac{B}{D}\right)} \quad (\text{A2})$$

$$B = \mu_e + 1.40 - 2.5 \log_{10}(7.22\pi r_e^2)$$

$$D = \mu_o - 2.5 \log_{10}(\pi \alpha^2),$$

where B is the magnitude of the bulge, and D is the magnitude of the disc. B/T is the bulge-to-total ratio. Given the parameters M , B/T , μ_e and μ_o , a galaxy's light profile is fully defined.

To calculate the difference between the total and the isophotal magnitude, it is necessary to find the fraction of light lost below the isophote. Since the intrinsic detection isophote varies with the redshift, this difference will be a function of redshift. For a variety of redshifts from $z = 0.001$ to 0.201 , the fraction of light under the isophote was calculated, by first converting the above magnitudes to apparent magnitudes, and the intrinsic surface brightnesses to apparent surface brightnesses, and then calculating the scale-lengths as above. The conversions from absolute to apparent properties are given in equations (17) and (18).

Using $\mu_{\text{lim}} = 24.67 \text{ mag arcsec}^{-2}$, the isophotal radii of the disc and bulge are calculated:

$$r_{\text{iso,d}} = \left(\frac{\mu_{\text{lim}} - \mu_o}{1.086} \right) \alpha$$

$$r_{\text{iso,b}} = \left[\frac{\mu_{\text{lim}} - (\mu_e + 1.40)}{8.325} + 1 \right]^4 r_e. \quad (\text{A3})$$

The fraction of light above the isophote is then calculated using the following equation:

$$f = 1 - \sum_{n=0}^{2\beta-1} \frac{1}{n!} g^n e^{-g}, \quad (\text{A4})$$

where β is the de Vaucouleurs parameter, which is 1 for a disc and 4 for a bulge. $g = 7.67(r/r_e)^{1/4}$ in bulges and $g = r/\alpha$ in discs. The isophotal magnitude and isophotal radius of the galaxy can now be calculated:

$$m_{\text{iso,b}} = m_b - 2.5 \log_{10} f_b$$

$$m_{\text{iso,d}} = m_d - 2.5 \log_{10} f_d$$

$$m_{\text{iso}} = -2.5 \log_{10}(10^{-0.4m_{\text{iso,b}}} + 10^{-0.4m_{\text{iso,d}}})$$

$$r_{\text{iso}} = \max(r_{\text{iso,b}}, r_{\text{iso,d}}) \quad (\text{A5})$$

Now that the isophotal magnitude, m_{iso} , has been found, it is possible to convert it back to an absolute magnitude, M_{iso} . The isophotal magnitude and radius are now fed back through the

³Note that the term 'effective surface brightness' is sometimes defined as the surface brightness at r_e ; for ellipticals the difference between these definitions of effective surface brightness is 1.40.

equations in Section 4, and a value of m^{corr} is calculated. This is converted to an absolute magnitude, and Table C4 shows a comparison of M_{true} , M_{iso} and M_{corr} at $z = 0.12$ for the main Hubble type galaxies and LSBGs. The properties of the LSBGs (B/T , μ_e and μ_o) come from averaging the B -band data in Beijersbergen, de Blok & van der Hulst (1999), and the values of B/T for S0, Sa, Sb and Sc galaxies are taken from Kent (1985). The μ_e values are taken from fig. 5 of Kent (1985) for ellipticals and spirals, extrapolating where necessary (i.e., for Sb, take a value between the median for Sa–Sb and Sbc+) and subtracting 1.40 for the conversion from the surface brightness at r_e to the effective surface brightness. For μ_o , we used the Freeman value for spiral discs (Freeman 1970). Irregular galaxies are usually placed beyond spirals on the Hubble sequence. They have either no bulge or a small bulge (van den Bergh 1998; Smoker, Axon & Davies 1999), and the majority are small $M_B > -17$. Ferguson & Binggeli (1994) show that all galaxies with $M_B > -16$ can be fitted with exponential profiles.

The absolute magnitude is kept constant at $M_{\text{true}} = -21$, and the values of M_{iso} and M_{corr} are calculated at $z = 0.12$. Adjusting the value of M_{true} does not affect the changes in magnitude at any particular redshift, but it does effect the maximum redshift at which the galaxy can be seen. The differences between M_{iso} and M_{true} and between M_{corr} and M_{true} both increase with redshift. In all cases except an elliptical galaxy, the value of M_{corr} is a *substantial* improvement over M_{iso} , and remains below the photometric error for all types out to $z = 0.12$.

APPENDIX B: VISIBILITY THEORY

The equations below are reproduced from Disney & Phillipps (1983) and Phillipps et al. (1990). They are used to calculate the volume over which a galaxy of absolute magnitude M and central surface brightness μ_o can be seen. The theory determines the maximum distance at which a galaxy can be seen, using two constraints: the apparent magnitude that the galaxy would have, and the apparent size that the galaxy would have. The first constraint sets a limit on the luminosity distance to the galaxy, which is the distance that a galaxy is at when it becomes too faint to be seen:

$$d_1 = [f(\mu_{\text{lim}} - \mu_o)]^{1/2} 10^{(0.2[m_{\text{lim}} - M - 25 - K(z)])} \text{ Mpc}, \quad (\text{B1})$$

where $f(\mu_{\text{lim}} - \mu_o)$ is the fraction of light above the isophotal detection threshold and is profile-dependent. For a spiral disc with an exponential profile, the fraction of light is

$$f(\mu_{\text{lim}} - \mu_o) = 1 - [1 + 0.4 \ln(10)(\mu_{\text{lim}} - \mu_o)] 10^{[-0.4(\mu_{\text{lim}} - \mu_o)]}. \quad (\text{B2})$$

The values of μ_{lim} and μ_o have both to be absolute or apparent for the above relation to be true. As the known value of μ_{lim} is the apparent value and the known value of μ_o is the absolute value, a redshift-dependent factor must be included in all calculations:

$$\mu_{\text{lim}} - \mu_o \rightarrow \mu_{\text{lim}}^{\text{app}} - \mu_o - 10 \log_{10}(1+z) - K(z). \quad (\text{B3})$$

Thus the maximum distance has a redshift dependence. The luminosity distance is a function of redshift:

$$d_L(z) = \frac{2c}{H_0} [(1+z) - (1+z)^{0.5}]. \quad (\text{B4})$$

The maximum distance can be found numerically by, for instance, a Newton–Raphson iteration as

$$d_1(z) - d_L(z) = 0 \quad (\text{B5})$$

at the maximum distance.

The second constraint, the size limit, is found by a similar methodology. The formulation of the size limit is

$$d_2 = Cg(\mu_{\text{lim}} - \mu_o)10^{[0.2(\mu_o - M)]} / \theta_{\text{lim}} \text{ Mpc}, \quad (\text{B6})$$

where C is a profile-dependent constant. $g(\mu_{\text{lim}} - \mu_o)$ is the isophotal radius in scalelengths. θ_{lim} is the minimum apparent diameter. For a spiral disc with an exponential profile

$$C = \frac{2}{\sqrt{2\pi}} 10^{-5} \quad (\text{B7})$$

$$g(\mu_{\text{lim}} - \mu_o) = 0.4 \ln(10)[\mu_{\text{lim}}^{\text{app}} - \mu_o - 10 \log_{10}(1+z) - K(z)]. \quad (\text{B8})$$

In this case d_2 is an angular-diameter distance, not a luminosity distance:

$$d_A(z) = \frac{2c}{H_0} [(1+z)^{-1} - (1+z)^{-1.5}] \quad (\text{B9})$$

$$d_2(z) - d_A(z) = 0. \quad (\text{B10})$$

Once the redshifts z_1 and z_2 , which are the solutions of equations (B5) and (B10), have been found, the maximum redshift at which the galaxy can be seen is the minimum of z_1 and z_2 :

$$z_{\text{max}} = \min(z_1, z_2). \quad (\text{B11})$$

For the 2dFGRS, the parameters above are $\mu_{\text{lim}} = 24.67 \text{ mag arcsec}^{-2}$, $m_{\text{lim}} = 19.45 \text{ mag}$, and $\theta_{\text{lim}} = 7.2 \text{ arcsec}$. $z_{\text{max}} \leq 0.12$ is another limit imposed on this survey.

There are also limits on the minimum redshift. These are also caused by selection effects in the survey. One limit comes from the maximum apparent brightness of galaxies in the sample, which is $m = 14.00$. The minimum redshift, z_3 , is calculated just as z_1 . There is also a maximum radius for galaxies, which is $\theta_{\text{max}} = 200 \text{ arcsec}$. This comes from the sky-subtraction process. This leads to z_4 , calculated in the same way as z_2 :

$$z_{\text{min}} = \max(z_3, z_4), \quad (\text{B12})$$

where $z_{\text{min}} \geq 0.015$. This limit is to prevent peculiar velocities dominating over the Hubble flow velocity. Also,

$$V(M, \mu_o) = \int_{z_{\text{min}}(M, \mu_o)}^{z_{\text{max}}(M, \mu_o)} \frac{\sigma c d_L^2}{H_0(1+z)^{3.5}} dz, \quad (\text{B13})$$

where σ is the area on the sky in steradians, c is the speed of light, and H_0 is Hubble's constant. The visibility $V(M, \mu_o)$ represents the volume over which a spiral disc galaxy of absolute magnitude M and central surface brightness μ_o can be observed. The central surface brightness can be converted to effective surface brightness using the following formula:

$$\mu_e = \mu_o + 1.124. \quad (\text{B14})$$

APPENDIX C: TABLES

Table C1. A comparison of the local luminosity density from recent magnitude-limited redshift surveys.

| Survey | Reference | M^* | ϕ^* | α | $j_B/10^8 h_{100} L_{\odot} \text{ Mpc}^{-3}$ |
|-------------------|--------------------------|--------|-----------------------|----------|---|
| SSRS2 | Marzke et al. (1998) | -19.43 | 1.28×10^{-2} | -1.12 | 1.28 |
| Durham/UKST | Ratcliffe et al. (1998) | -19.68 | 1.7×10^{-2} | -1.04 | 2.02 |
| ESP | Zucca et al. (1997) | -19.61 | 2.0×10^{-2} | -1.22 | 2.58 |
| LCRS* | Lin et al. (1996) | -19.19 | 1.9×10^{-2} | -0.70 | 1.26 |
| EEP | Efstathiou et al. (1988) | -19.68 | 1.56×10^{-2} | -1.07 | 1.89 |
| Stromlo/APM | Loveday et al. (1992) | -19.50 | 1.40×10^{-2} | -0.97 | 1.35 |
| Autofib | Ellis et al. (1996) | -19.20 | 2.6×10^{-2} | -1.09 | 2.05 |
| CfA ^{*2} | Marzke et al. (1994) | -19.15 | 2.4×10^{-2} | -1.00 | 1.71 |

* The LCRS used a Gunn r filter. The value of M^* has been converted to M_B using $\langle b_j - R \rangle_o = 1.1$ for the Johnson B band (Lin et al. 1996). ^{*2} The CfA used Zwicky magnitudes. The value of M^* has been converted to M_B using $\langle b_j - M_Z \rangle_o = -0.35$ for the Johnson B band, and ϕ^* has been reduced by 60 per cent (Gaztanaga & Dalton 2000).

Table C2. A table of the number density as a function of M and μ_c for the 2dFGRS data. The values are in units of 1.0×10^{-4} galaxies Mpc^{-3} . The dashes are in bins where visibility theory says that the volume sampled $V(M, \mu) < 10^4 \text{Mpc}^3$. The bold numbers are in bins where there are more than 25 galaxies. The italic numbers are in bins where there are less than 25 galaxies and visibility theory is used to calculate the number density. Where this becomes less than 1 galaxy in 10^4Mpc^3 , the limit <1 is used.

| Bin | 20.1 | 20.6 | 21.1 | 21.6 | 22.1 | 22.6 | 23.1 | 23.6 | 24.1 | 24.6 |
|-------|------------|------------------|------------------|------------------|------------------|------------------|------------------|------------------|------------|------|
| -24.0 | - | - | - | <1 | <1 | <1 | <1 | <1 | <1 | <1 |
| -23.5 | <1 | <1 | <1 | <1 | <1 | <1 | <1 | <1 | <1 | <1 |
| -23.0 | <1 | <1 | <1 | <1 | <1 | <1 | <1 | <1 | <1 | <1 |
| -22.5 | <1 | <1 | <1 | <1 | <1 | <1 | <1 | <1 | <1 | <1 |
| -22.0 | <1 | <1 | <1 | <1 | <1 | <1 | <1 | <1 | <1 | <1 |
| -21.5 | <1 | <1 | <1 | 1.4 ± 0.4 | <1 | <1 | <1 | <1 | <1 | <1 |
| -21.0 | <1 | <1 | 4.2 ± 0.6 | 6.1 ± 0.8 | 3.3 ± 0.6 | <1 | <1 | <1 | <1 | <1 |
| -20.5 | <1 | 1.9 ± 0.4 | 8.8 ± 0.9 | 18 ± 1.3 | 12 ± 1.1 | 3.0 ± 0.5 | <1 | <1 | <1 | <1 |
| -20.0 | <1 | 2.9 ± 0.7 | 14 ± 1.2 | 42 ± 2.0 | 33 ± 1.8 | 9.0 ± 0.9 | <1 | <1 | <1 | <1 |
| -19.5 | <1 | <1 | 15 ± 1.2 | 59 ± 2.4 | 65 ± 2.5 | 26 ± 1.6 | 5.7 ± 0.8 | <i>1.3</i> | <1 | <1 |
| -19.0 | <1 | <i>1.0</i> | 13 ± 1.4 | 58 ± 2.4 | 98 ± 3.1 | 52 ± 2.4 | 14 ± 1.4 | 4.2 ± 1.0 | <1 | <1 |
| -18.5 | <1 | <1 | 11 ± 1.7 | 61 ± 3.5 | 111 ± 4.4 | 77 ± 3.7 | 35 ± 2.8 | 11 ± 1.9 | <i>3.0</i> | <1 |
| -18.0 | <1 | <1 | 15 ± 4.1 | 43 ± 3.5 | 110 ± 5.8 | 113 ± 6.0 | 55 ± 4.6 | 21 ± 3.4 | <i>2.7</i> | <1 |
| -17.5 | <1 | <1 | <i>2.8</i> | 31 ± 4.4 | 96 ± 7.4 | 126 ± 8.6 | 62 ± 6.7 | 35 ± 6.9 | <i>7.1</i> | <1 |
| -17.0 | <i>2.5</i> | <i>1.6</i> | <i>2.2</i> | 39 ± 8.9 | 113 ± 13 | 136 ± 14 | 103 ± 14 | 44 ± 10 | <i>20</i> | <1 |
| -16.5 | - | <1 | <i>2.3</i> | <i>27</i> | 101 ± 16 | 151 ± 19 | 116 ± 17 | 66 ± 14 | <i>30</i> | - |
| -16.0 | - | - | - | <i>19</i> | 50 ± 14 | 171 ± 27 | 130 ± 24 | <i>72</i> | - | - |
| -15.5 | - | - | - | - | - | 126 ± 34 | <i>102</i> | - | - | - |
| -15.0 | - | - | - | - | - | - | - | - | - | - |
| -14.5 | - | - | - | - | - | - | - | - | - | - |

Table C3. A summary of the luminosity densities and upper limits on Ω_M found from the 2dFGRS data.

| Parameters | $j/10^8 h L_\odot \text{Mpc}^{-3}$ | Ω_M |
|----------------------------|------------------------------------|-----------------|
| $\mu_{\text{lim}} = 24.67$ | 2.49 ± 0.20 | 0.24 ± 0.05 |
| $\mu_{\text{lim}} = 24.97$ | 2.33 ± 0.17 | 0.23 ± 0.05 |
| $\mu_{\text{lim}} = 24.37$ | 3.00 ± 0.26 | 0.29 ± 0.06 |
| Simple LF | 1.82 ± 0.09 | 0.18 ± 0.04 |

Table C4. A summary of the errors in the isophotal and corrected magnitudes.

| Hubble Type | M_{true} | BIT | μ_c | μ_o | M_{iso} | M_{corr} |
|-------------|-------------------|-------|---------|---------|------------------|-------------------|
| E | -21.00 | 1.00 | 20.5 | - | -21.00 | -21.07 |
| S0 | -21.00 | 0.65 | 19.2 | 21.7 | -20.83 | -20.89 |
| Sa | -21.00 | 0.50 | 19.6 | 21.7 | -20.75 | -20.86 |
| Sb | -21.00 | 0.30 | 20.4 | 21.7 | -20.64 | -20.86 |
| Sc | -21.00 | 0.15 | 21.0 | 21.7 | -20.54 | -20.89 |
| Sd | -21.00 | 0.10 | 21.2 | 21.7 | -20.51 | -20.92 |
| LSBG | -21.00 | 0.12 | 27.7 | 23.0 | -19.08 | -20.84 |
| Irr | -21.00 | 0.00 | - | 22.7 | -19.67 | -21.00 |

This paper has been typeset from a $\text{\TeX}/\text{\LaTeX}$ file prepared by the author.